Available online at www.sciencedirect.com
ScienceDirect
Soils and Foundations 65 (2025) 101536
www.elsevier.com/locate/sandf

Technical Paper

Study on long-term subsidence of soft clay due to Niigata-ken Chuetsu-oki earthquake of 2007

Yazhou Jiang[a,*], Koichi Isobe[b], Satoru Ohtsuka[c], Toshiyuki Takahara[d]

[a] Division of Field Engineering for Environment, Hokkaido University, Sapporo, Japan
[b] Division of Civil Engineering, Hokkaido University, Sapporo, Japan
[c] Department of Civil and Environmental Engineering, Nagaoka University of Technology, Nagaoka, Japan
[d] Department of Civil and Environmental Engineering, Kanazawa Institute of Technology, Kanazawa, Japan

Received 7 September 2023; received in revised form 27 September 2024; accepted 1 November 2024
Available online 19 December 2024

Abstract

In the Niigata-ken Chuetsu-oki Earthquake of 2007, ground liquefaction was outstanding at the foot of a sand dune and in old river channels. Although no distinct disaster was found in the clayey ground after the earthquake, the long-term settlement of the ground was observed after the earthquake in the Shinbashi district of Kashiwazaki City. At one observation site, the cumulated ground subsidence of the layers from the ground surface to a depth of 23 m had reached 71 mm 14 years after the earthquake. In order to study the mechanism of the deformation during the earthquake and the long-term settlement after the earthquake, ground investigations, such as a boring survey at the observation site and indoor element tests on sampled soil, were conducted in this study. The results showed that the sampled soil was very soft, strongly compressible, and relatively highly structured. Subsequently, the transformation stress-cyclic mobility (TS-CM) constitutive model, developed by Zhang et al. (2007), was used to simulate the results of the indoor element tests, and the soil parameters were determined based on the results of these tests. The TS-CM model contains the concepts of subloading, described by Hashiguchi (1977), and superloading, described by Asaoka et al. (2002). Therefore, the subsidence behavior of the ground was simulated by a soil–water coupling elasto-plastic finite element (FE) analysis using the TS-CM constitutive model and the determined parameters. The FE simulation results agreed well with the actual site subsidence observation data. Based on the simulation results, the post-earthquake behavior of the soft clay and its mechanism were discussed, and the successive subsidence was predicted forward. According to the simulation results, the relatively highly structured susceptible clay at this site was found to have greater potential in terms of long-term consolidation than relatively less structured susceptible clay due to the large excess pore water pressure generation during the ground motion and the consolidation process after the earthquake. This conclusion was verified by consolidation tests on two types of clay.

Keywords: Post-earthquake settlement; Structured clay; FE analysis; Tri-axial test; Structure degradation

1. Introduction

The Niigata-ken Chuetsu-oki Earthquake of 2007, that hit Japan on July 16th, killed 11 people and damaged more than 1,000 houses. The quake registered 6.8 on the magnitude scale of the Japan Meteorological Agency (JMA), and a Kyoshin Net (K-NET) accelerograph measured a maximum value of 680 Gal. A maximum seismic intensity of 6

* Corresponding author.
E-mail addresses: yzjiang830@yahoo.com, yazhou.jiang.z8@elms.hokudai.ac.jp (Y. Jiang), kisobe@eng.hokudai.ac.jp (K. Isobe), ohtsuka@vos.nagaokaut.ac.jp (S. Ohtsuka).

https://doi.org/10.1016/j.sandf.2024.101536

upper was measured in Kashiwazaki City, as presented in Fig. 1. As seen in Figs. 2 and 3, many houses were damaged, and some types of ground deformation, such as liquefaction, were observed in Kashiwazaki City (Isobe et al., 2014a) and Kariwa Village. In the Hashiba district of Kashiwazaki City and in Kariwa Village, foundation damage to timber houses and ground deformation were extensively observed. Therefore, a lot of attention was paid to house damage due to the liquefaction at the foot of a sand dune and in old river channels brought about by the earthquake. Conversely, it was thought that the house damage on the Kashiwazaki Plane, which consists of alluvial soft clay, was relatively less severe than that due to liquefaction. However, it was clarified from the results of the ground subsidence measured by Niigata Prefecture in the Shinbashi district of Kashiwazaki City that the ground subsidence continued over a lengthy period after the quake (Ohtsuka et al., 2021).

The same phenomena were observed in the 1957 Mexico Earthquake, the 1978 Miyagi-ken-oki Earthquake, the 1985 Mexico Earthquake, the 1995 Hyogo-ken Nanbu Earthquake, and the 2011 off the Pacific coast of Tohoku Earthquake which were reported by Zeevaert (1973), Suzuki (1984), Jaime et al. (1987), Matsuda (1997), Yasuhara et al. (1982), Nigorikawa et al. (2015), and Sento (2020). Particularly, in the classic example of the Mexican Earthquake, the post-earthquake settlement of the soft soil layer, which is located relatively far from the epicenter, was very significant (Ovando-Shelley et al., 2013; Avilés et al., 2010; Albano et al., 2016). Occurrences of similar cases have often been associated with the deposition of a thick layer of soft alluvial clay. The present research holds significance because this phenomenon will greatly impact the maintenance and management of various buried pipes and pile foundations.

Based on these findings, much attention has been paid to decreasing the effective stress and the reconsolidation of saturated clay induced by cyclic shearing, and the outcome of such research has been published by Yasuhara et al. (1982), Hyodo et al. (1988), Ohara and Matsuda (1988), Matsuda and Ohara (1990), Yasuhara and Andersen (1991), Hyodo et al. (1992), Matsuda and Nagira (2000),

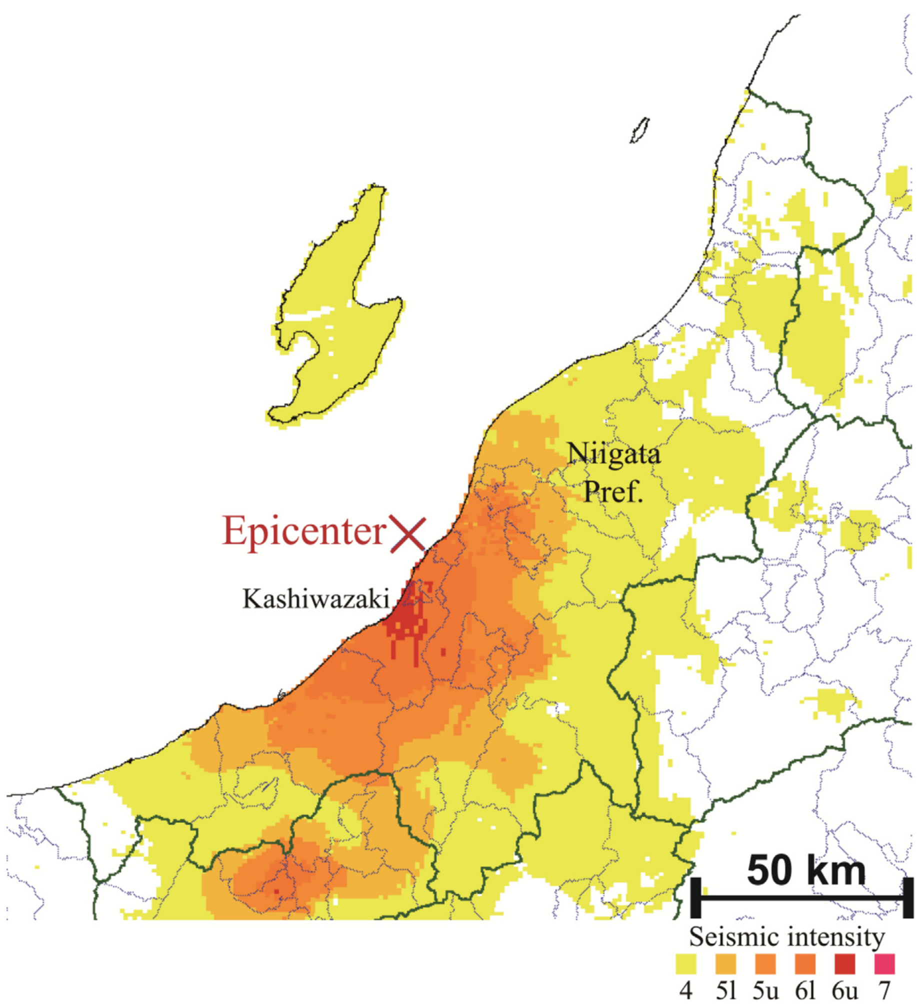

Fig. 1. Seismic intensity distribution map of 2007 Niigata-ken Chuetsu-oki Earthquake.

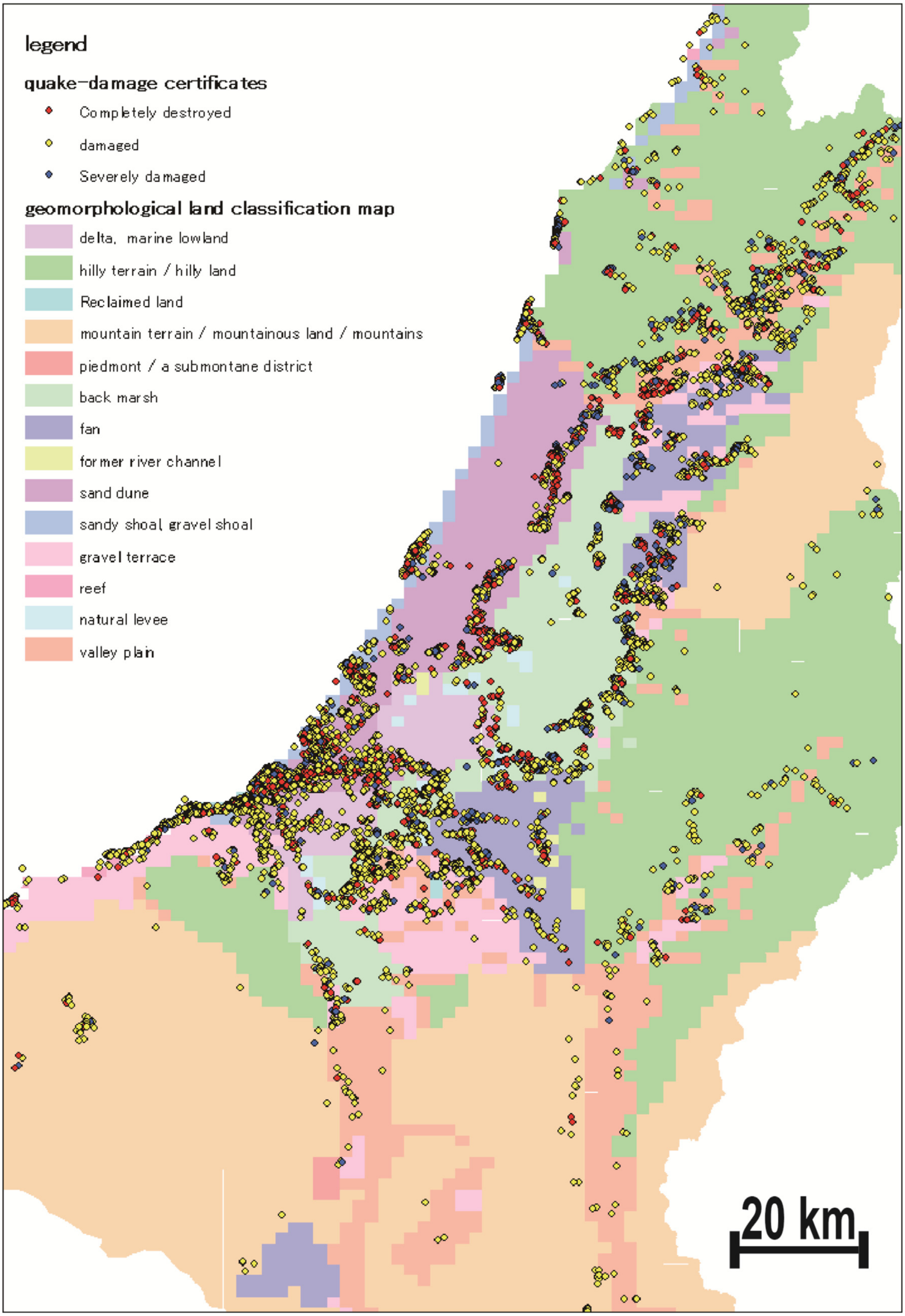

Fig. 2. Distribution map showing residential damage in Kashiwazaki City and Kariwa Village, due to 2007 Niigata-ken Chuetsu-oki Earthquake, and geomorphological land classification.

Fig. 3. Earthquake damage in Matsunami district of Kashiwazaki City: (a) most severely damaged house, (b) damaged houses due to ground crack, and (c) sand boiling (Isobe et al., 2014a).

and so on. Generally speaking, the change in void ratio Δe, produced in the soil mass, is in proportion to the logarithm of the effective stress. The relation between Δe and the logarithm of the increment in effective stress $\Delta \log p'$ or $\Delta \log s_v'$ is shown in Fig. 4, where C_c and C_s are the compression index and swelling index, respectively, obtained by standard oedometer tests. In the foregoing references, the relationship among both indexes and the compression index induced by dynamic loading C_d is shown as $C_s < C_d < C_c$. Based on this relationship, various experimental estimation methods for the post-earthquake settlement of clay layers have been proposed.

On the other hand, remarkable development has been realized for many simulation techniques. In particular, research on constitutive models for soils has been developing very quickly. The term initial anisotropy was firstly proposed to describe the phenomenon of anisotropy by Sekiguchi (1977). Then, Hashiguchi and Chen (1998)

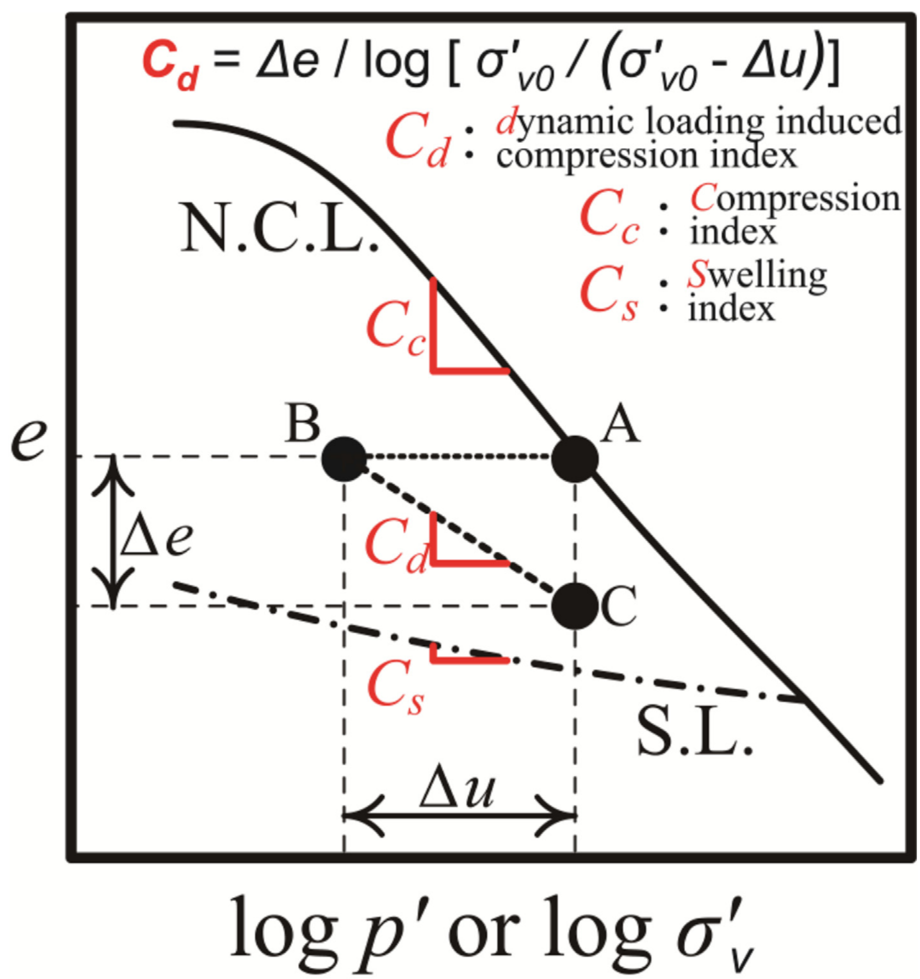

Fig. 4. Schematic view of C_c, C_s, and C_d.

proposed a rotation tensor to describe stress-induced anisotropy. The concept of subloading, proposed by Hashiguchi and Ueno (1977) and Hashiguchi (1978, 1989), has made it possible to describe the over-consolidation of soils easily and efficiently. The concept of superloading, proposed by Asaoka et al. (1994), Asaoka et al. (2000a), and Asaoka et al. (2000b), together with the concept of subloading, has made it possible not only to describe over-consolidation, but also to explain the effect of the soil structure commonly observed in naturally deposited soils. By combining the concepts of subloading and superloading, it is possible for the first time to describe the mechanical behavior of clay and sand with different densities and different structures within the same framework of a constitutive model. The proposed model is based on the Cam-clay model (Roscoe et al., 1963) and the modified Cam-clay model (Schofield and Worth, 1968). Therefore, the physical meaning of the model is easy to understand, and relatively few parameters are needed despite its ability to deal with different soils using the same model. Based on the proposed model, Kaneda et al. (2003) explained the behavior of delayed compression observed in land subsidence, brought about by dewatering, and pointed out the importance of the compression-softening behavior of naturally deposited soils. Moreover, a new approach for describing stress-induced anisotropy and a new evolution rule for changes in over-consolidation were proposed based on the aforementioned concepts by Zhang et al. (2007). In the approach, the mechanical behavior of soils subjected to cyclic loading under undrained conditions, including the cyclic mobility of medium dense sand, is examined. Furthermore, valuable research on liquefaction analysis (Mase et al., 2022), seismic wave amplification (Qodri et al., 2021), and ground response analysis (Mase et al., 2020, 2021; Likitlersuang et al., 2020) has been conducted.

In the present research, a boring investigation, comprising standard penetration tests (SPT), was conducted near the observation point of the ground subsidence in Kashiwazaki City in order to investigate the cause of the long-term subsidence of soft clay induced by the earthquake. Static and cyclic consolidated undrained (CU) tri-axial tests were carried out to clarify the mechanical characteristics and liquefaction strength of Kashiwazaki clay. Subsequently, a numerical analysis was carried out to simulate the observed subsidence using a soil–water coupling elasto-plastic finite element (FE) analysis with soil parameters that were determined based on the above element test results. In the present paper, the cause of the long-term subsidence of soft clay was discussed and the amount of future subsidence was mathematically predicted based on the simulation results.

2. Overview of geographical conditions in Kashiwazaki city

Fig. 5(a), (b), and (c) present terrain classification, altitude distribution, and geological cross section maps for the city. The areas where ground subsidence was observed before the earthquake are mainly located on land which consists of soft alluvial clay. On the other hand, the areas where ground subsidence rapidly increased after the quake are located near the seaside and are mostly covered by the above-mentioned soft alluvial clay. The local geological characteristics of these areas were reported in detail by Ohtsuka et al. (2021). The stratified subsidence and ground water level were measured by Niigata Prefecture in the Shinbashi district of Kashiwazaki City, labeled Point B in Fig. 5, from 1989 to 2022. Fig. 6 shows the temporal changes in both the ground water level and the amount of ground subsidence of the soil layers to a depth of 23 m observed from 2005 to 2022. The measurement period for the ground water level and subsidence data in the figure is once a month in most of the years. It is found from the figure that the subsidence increased rapidly after the quake of 2007 and continued for a period of over 10 years. It was not caused by the consolidation of the soft clay due to changes in the ground water level because no drastic changes in the ground water level were observed there. Both the Niigata Earthquake of 1964 and the Chuetsu Earthquake of 2004 impacted this region historically. However, compared to the Chuetsu-oki Earthquake of 2007, the epicenter of the 2004 Chuetsu Earthquake was more distant, with a slightly lower recorded seismic intensity. Therefore, following the 2004 Chuetsu Earthquake, no long-term post-earthquake consolidation subsidence was observed in the clay ground. No ground subsidence observation was conducted around the 1964 Niigata earthquake, thereby creating uncertainty regarding the subsequent long-term consolidation subsidence. Hence, studying the long-term settlement phenomenon resulting from the 2007 earthquake is warranted.

In order to investigate the cause, a boring investigation involving standard penetration tests (SPT) was carried out near the observation point of the ground subsidence, and the soft clay in this area was sampled. Fig. 7 shows the geological columns in the city obtained from the boring investigation conducted by the authors and from the database of the Hokuriku Geological System. The land in the Shinbashi district mainly consists of very soft clay with an N-value of 0 to 2. Mixing small pieces of weathered shells from the vicinity of a depth of 11.0 m and the significant contamination from a depth close to 14.0 m can be confirmed. The soft clay layer exists up to a depth of 21 m and is underlaid by a silt layer having an N-value of approximately 10. The silt layer exists up to a depth of 50 m and has an N-value of more than 50 which is regarded as an engineering foundation ground. In contrast, the thickness of the soft clay layer in the area around the district of Point D is relatively less than that in the area around the district of Point C. A sand dune with an N-value of more than 10 covers the clay and silt layer at Point A near the seaside. It is clarified that the area where a lot of subsidence was observed after the quake corresponds to the area which consists of a thick alluvial clay layer.

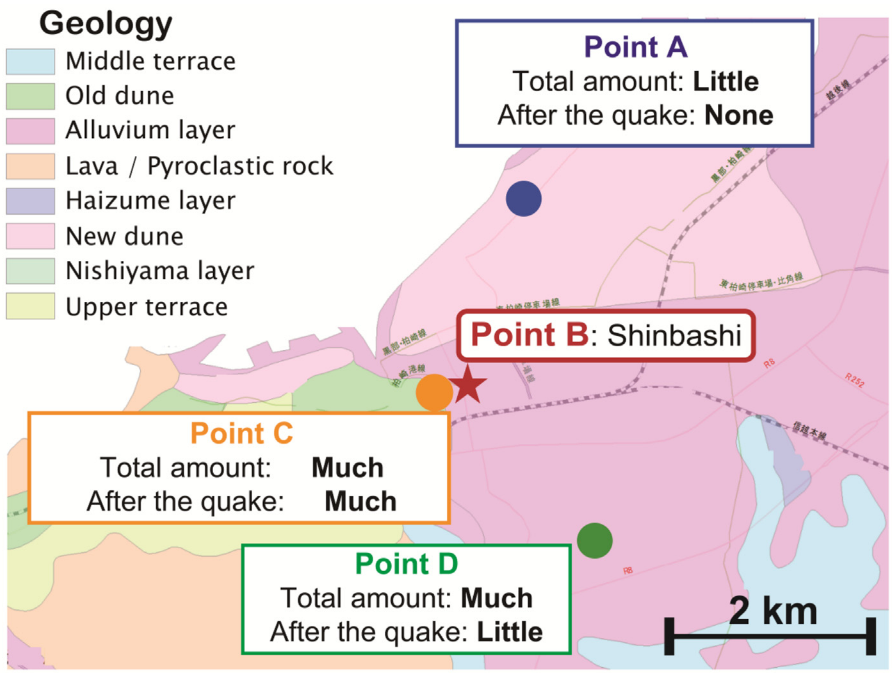

Fig. 5. (a) Terrain classification map for Kashiwazaki City (Ohtsuka et al., 2021). (b) Altitude distribution map for Kashiwazaki City (Ohtsuka et al., 2021). (c) Geological cross section map for Kashiwazaki City (Ohtsuka et al., 2021).

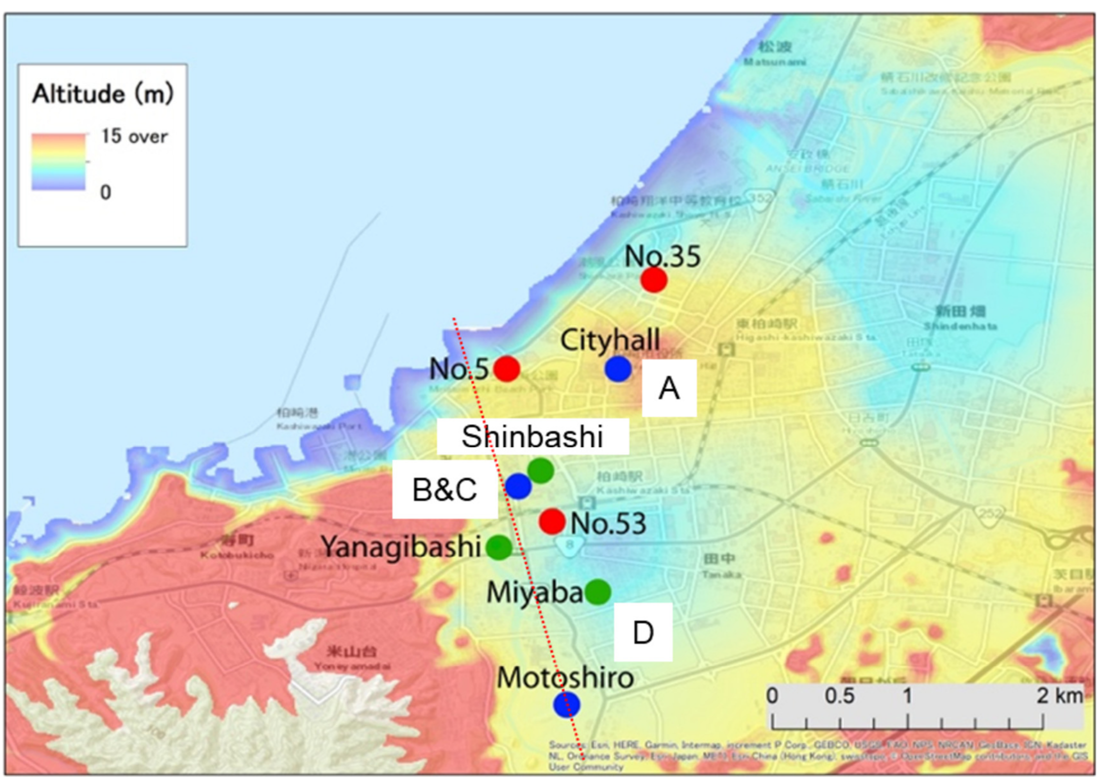

Fig 5. *(continued)*

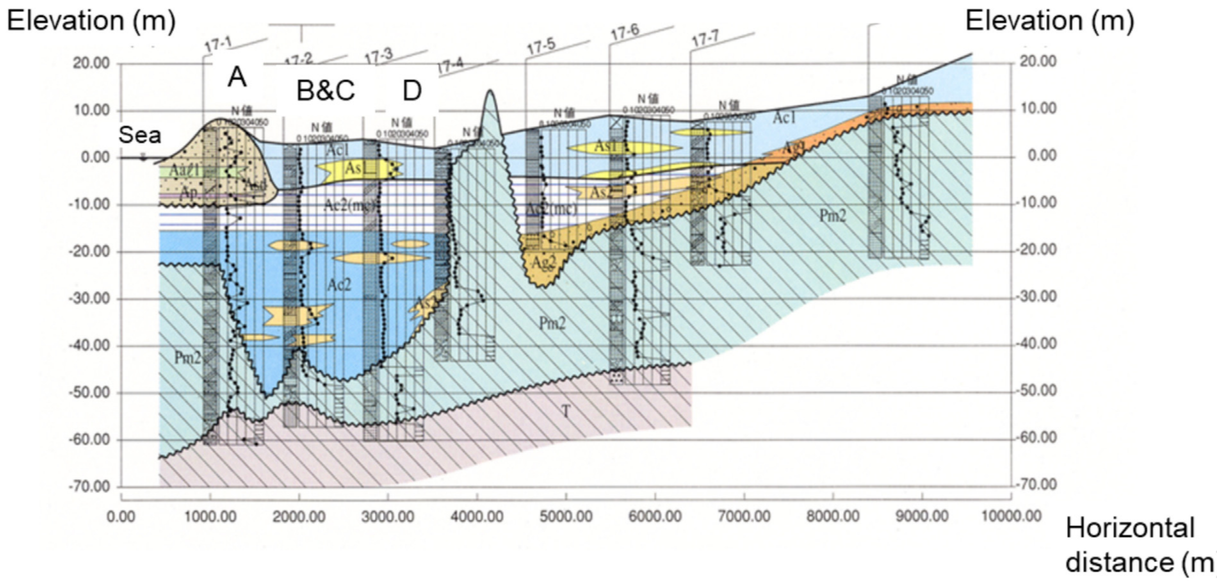

Fig 5. *(continued)*

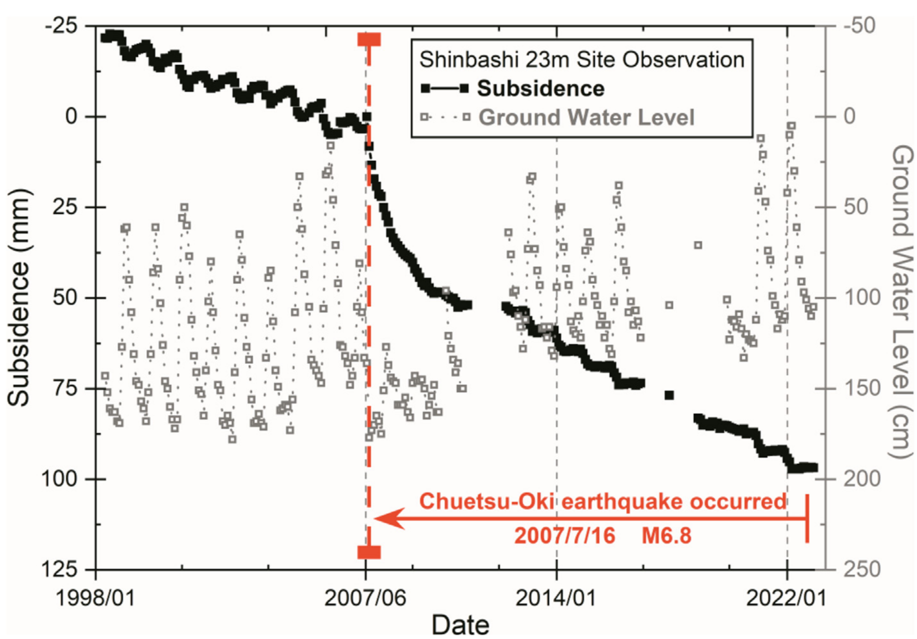

Fig. 6. Temporal changes in ground water level and cumulated subsidence of soil layers to depth of 23 m (from 2005 to 2022).

3. Physical properties and mechanical characteristics of sampled soft clay

3.1. Physical properties and consolidation test results

As there is a difference in the amount of contamination in the weathered shells between the shallow clay layer and the deep clay layer, intact samples were obtained from the layer between the depths of G.L. −7 and 21 m in the Shinbashi district of Kashiwazaki City using a small diameter sampler with a two-chambered hydraulic piston developed by Shogaki and Sakamoto (2004) to conduct oedometer tests, static CU tests, and cyclic CU tests. Lateral load tests (LLTs) were also conducted at the same site. The physical properties and LLT results for the deep clay layer in the Kashiwazaki City clay are shown in Tables 1 and 2, respectively. The grain size distribution curve for the deep clay layer is shown in Fig. 8. It is confirmed that the deep clay has a high natural water content and plasticity index, and consists of more than 50 % clay, which points to a greater probability of large settlement. This explains why relatively large post-earthquake subsidence occurred in the Kashiwazaki area covered with soft clay.

Subsequently, some oedometer tests were performed to clarify the consolidation characteristics of several samples. The following two types of specimens were created for the

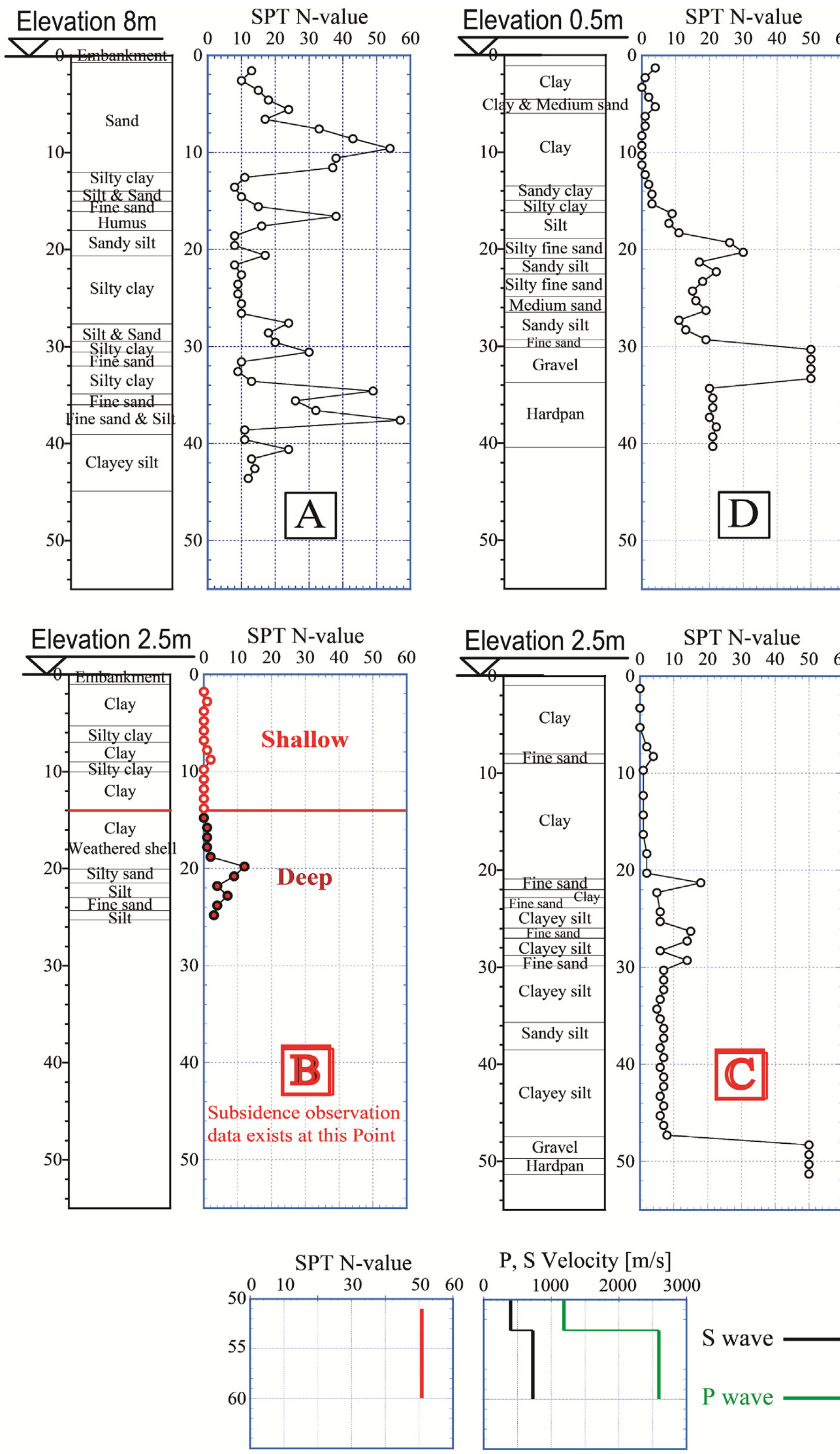

Fig. 7. Geological columns and wave velocity of Kashiwazaki City obtained from boring investigation carried out by authors and from database of (Hokuriku Geological System) (Points A ~ D correspond to areas on the map shown in Fig. 5).

oedometer tests: (1) an intact specimen and (2) a reconstituted specimen made from a slurry sample plus water after the above tests. Fig. 9 shows the results of the tests conducted on the intact and reconstituted samples from the shallow and deep layers and a thin transitional part. The reason for determining the existence of a transitional part is that the soil at a depth of 16 m showed significantly different behavior in the tests compared to that at other loca-

Table 1
Physical properties of deep clay sampled in Kashiwazaki City.

		Clay
Specific gravity [g/cm^3]	G_s	2.68
Plasticity index [%]	I_p	48.6
Liquid limit [%]	w_l	87.0
Plastic limit [%]	w_p	38.4
Natural water content [%]	w_n	73.5

Table 2
Results of lateral load tests at Point B in Shinbashi district of Kashiwazaki City.

		Shallow layer	Deep layer
Depth [m]	D	9.0	17.0
Earth pressure at rest [kN/m^2]	P_0	24.7	48.5
Yield pressure [kN/m^2]	P_y	56.4	74.0
Destruction pressure [kN/m^2]	P_l	79.3	137.5
Deformation modulus [MN/m^2]	E	0.77	1.10
Subgrade modulus [MN/m^3]	K	14.34	19.98
SPT N-value	N	2	1

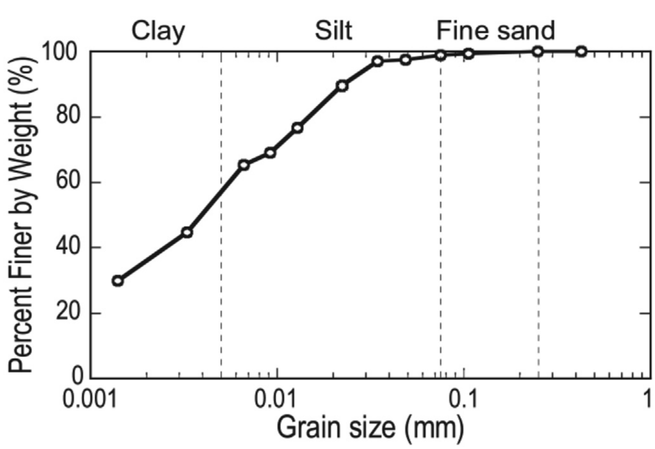

Fig. 8. Grain size distribution curve for deep clay layer.

tions, while various tests in the deep soil were done on the S-7, S-8, and S-9 samples below a depth of 17 m. However, the abnormal behavior of these single depth samples does not affect the overall trend. It implies that the intact samples from each layer have high compression characteristics after the application of consolidation yield pressure of about 80 kPa compared with those of the reconstituted samples. According to Asaoka et al. (2002), the clay obtained from the deep layer was identified as a slightly structured clay. In addition, it is inferred that the layers in the vicinity of the ground surface at the site were over-consolidated since the consolidation yield stress of both samples was around 70–90 kPa. After comparing the three intact specimen oedometer lines of the shallow layer clay and deep layer clay, it can be seen that the shallow layer clay has less potential to consolidate than the deep layer clay, which will also be important in subsequent analyses.

3.2. Static and cyclic tri-axial compression tests

Static and cyclic CU tri-axial tests were carried out on the Kashiwazaki clay to clarify the static and cyclic shear characteristics and the liquefaction strength of the clay. Two types of specimens were also created for the tri-axial compression tests: (1) a sampled intact specimen and (2) a reconstituted specimen formed by a slurry sample plus water in the above-mentioned test samples with a pre-consolidation method. The specimens were formed to be 5 cm in diameter and 10 cm in height. Table 3 shows the testing conditions of the static and cyclic CU tri-axial tests. The test apparatus consisted of a tri-axial cell, cell-pressure and back-pressure control devices, an axial load control device, and a data acquisition/recording system to collect data on the axial load, axial displacement, and pore water pressure of the specimens, as well as on the volume reduction during consolidation (i.e., water drainage from the specimens). Vacuum conditions were applied to both the cell and the sample interior to achieve a high degree of saturation. To ensure specimen saturation, the degree of saturation was evaluated at this stage based on the B-value until the B-value of the specimen was equal to or greater than 0.95. The specimen was isotopically consolidated for 18 h under a confining pressure of 50–200 kPa. The deep clay specimens, S-7, S-8, and S-9, were taken from depths of 17–19 m, while the shallow clay specimens, S-1, S-3, and S-5, were taken from depths of 7–12 m. In order to examine the static shear strength and liquefaction strength, static and cyclic tests were performed by applying deviator stress at a loading rate of 0.021 mm/min and uniform sinusoidal cycles of deviator stress at a frequency of 0.01 Hz with a varying cyclic stress ratio under constant cell pressure. The axial loads were measured using a load cell with a capacity of 5 kN installed between the top cap of the pedestal and the piston in the cell, and the axial strain was monitored using a displacement transducer outside the cell. The electrical outputs collected from the load cell, displacement transducer, pore water pressure transducer, and gap sensor, for the measurement of the decrease in specimen volume during consolidation, were amplified and recorded simultaneously using a computer.

Fig. 10 shows the relationships between the deviator stress and axial strain, and the deviator stress and mean effective stress paths, obtained from the static CU tri-axial tests for the intact specimens sampled from both layers. In the case of the deep layer samples under any confining pressure, mean effective stress p' is seen to decrease with the increase in excess pore water pressure (EPWP), but afterwards the p' of the sample under the confining pressure of 150 kPa increases a little along the critical state line (C.S.L.), while the p' of the samples under the confining pressures of 50 and 100 kPa is seen to continue decreasing along the C.S.L. When the stress path reaches the C.S.L., the deviator stress q of the samples from the shallow layer is higher than that of the samples from the deep layer subjected to the same confining pressure loading.

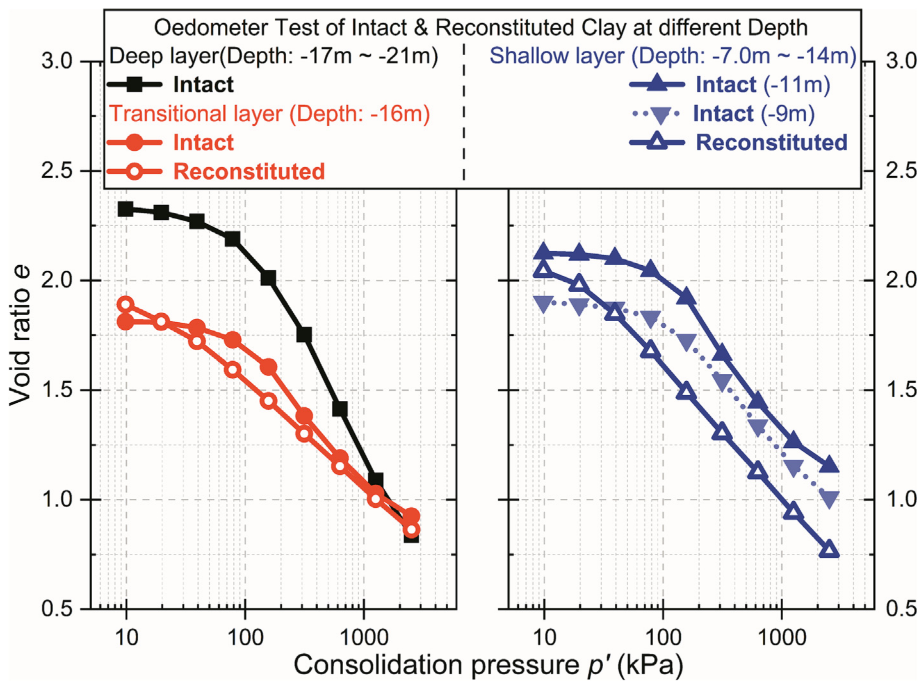

Fig. 9. Results of oedometer tests on intact and reconstituted samples.

Table 3
Testing conditions for static and cyclic triaxial compression tests.

		Shallow layer		Deep layer	
Sample type		Intact	Reconstituted	Intact	Reconstituted
Preconsolidation method			Iso. consol.		Iso. consol.
Initial void ratio of intact samples	e_0	1.91 ~ 2.13		1.82 ~ 2.34	
Effective confining pressure [kPa]	p'_0	50, 100, 150, 200	50, 100, 150	50, 100, 150	50, 100, 150
Back pressure [kPa]	B.P.	100	100	100	100
Drained condition		Undrained			
Static loading speed [%/min] (Strain control)		0.021			
Dynamic loading frequency [Hz]	f	N/A	N/A	0.01	N/A
Cyclic stress ratio (Stress control)	$\sigma_d/2\sigma'_0$	N/A	N/A	14.34	N/A

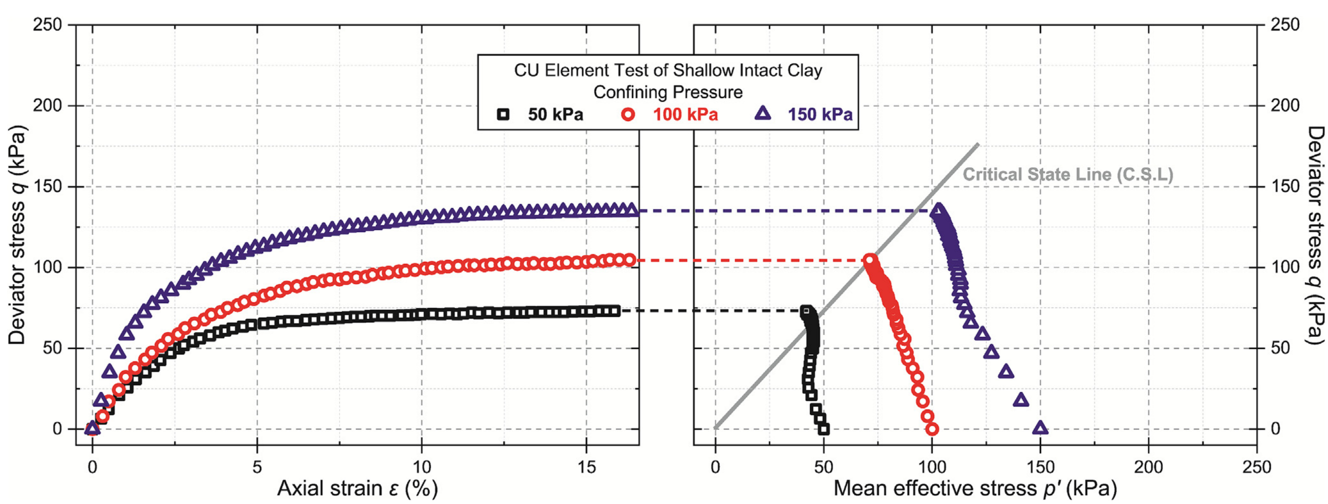

Fig. 10. (a) Results of static CU triaxial compression tests on intact samples from shallow layer. (b) Results of static CU triaxial compression tests on intact samples from deep layer.

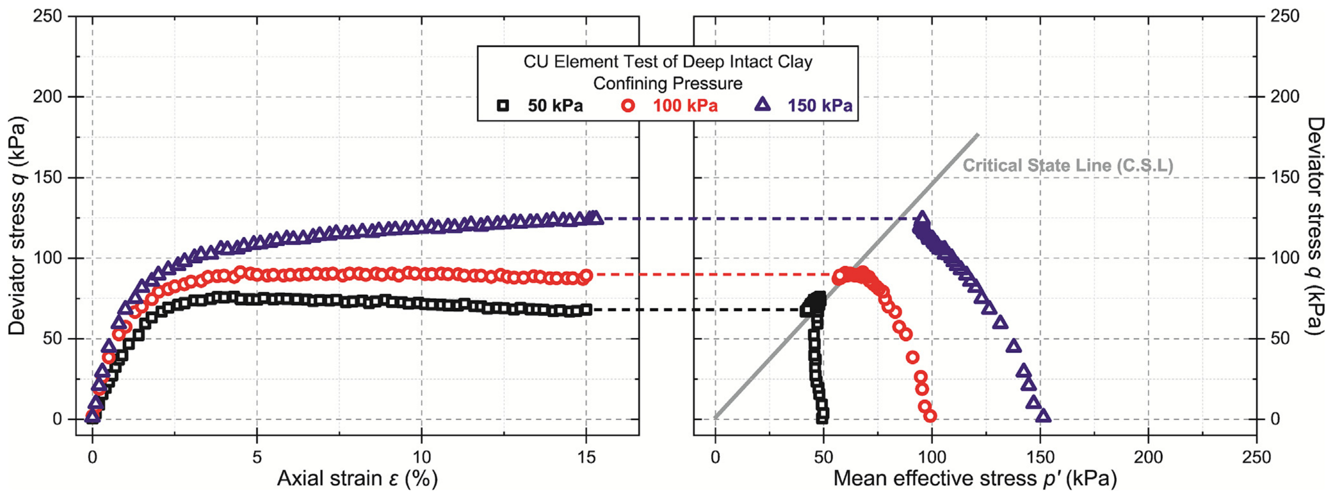

Fig 10. *(continued)*

Fig. 11 shows the relationships between the deviator stress and axial strain, and the deviator stress and mean effective stress paths, obtained from the cyclic CU triaxial compression/extension tests for the deep layer. Fig. 11(d) shows the liquefaction strength for the intact samples from the deep layer. The figure infers that the cyclic shear stress produces the EPWP. The liquefaction strength is defined as the cyclic stress ratio by which the double axial (DA) strain reaches 5 % under the cyclic number of 20. The liquefaction strength of the samples is 0.37. Although this value is greater than that of typical loose sand, it is natural that the clay layer is assumed to be sheared and that the EPWP increases during an earthquake.

4. Numerical simulation

4.1. Constitutive model used in simulation

The transformation stress-cyclic mobility (TS-CM) model developed by Zhang et al. (2007), which contains the concepts of subloading and superloading as described in the work by Hashiguchi and Ueno (1977) and Asaoka et al. (2002), is used for the constitutive model in this study. An illustration of the yield surfaces of the TS-CM model is given in Fig. 12.

The similarity ratio of the superloading surface to normal yield surface R^* and the similarity ratio of the superloading surface to subloading surface R are the same as those in the work by Asaoka et al. (2002), namely,

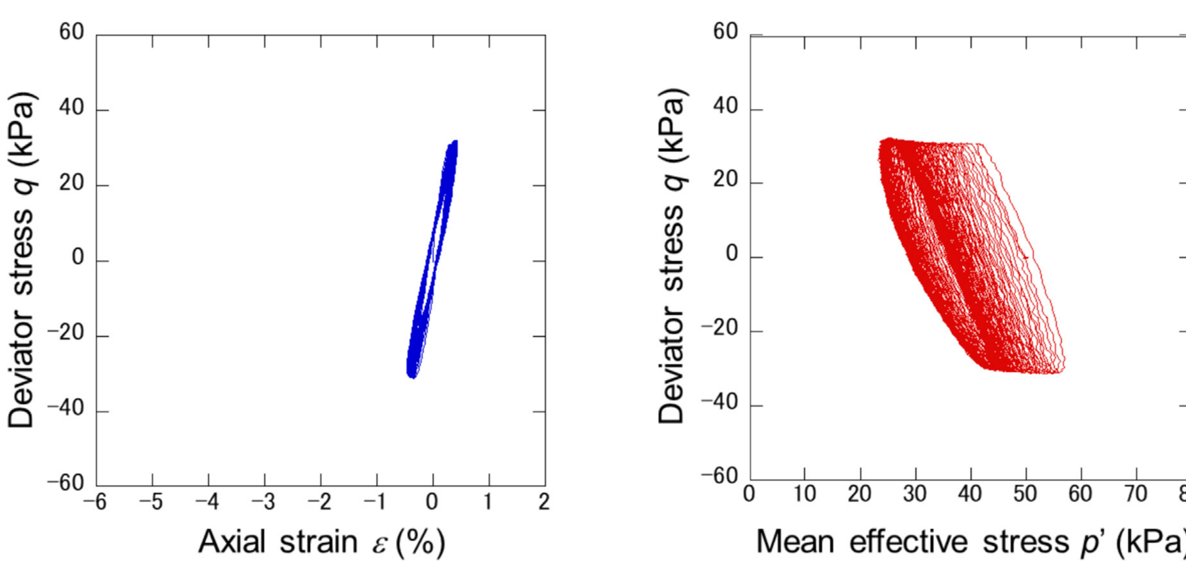

Fig. 11. (a) Results of cyclic triaxial tests on intact samples from deep layer ($\sigma_d / 2\sigma'_0 = 0.3$). (b) Results of cyclic triaxial tests on intact samples from deep layer ($\sigma_d / 2\sigma'_0 = 0.4$). (c) Results of cyclic triaxial tests on intact samples from deep layer ($s_d / 2\, s'_0 = 0.5$). (d) Liquefaction strength for intact samples from deep layer.

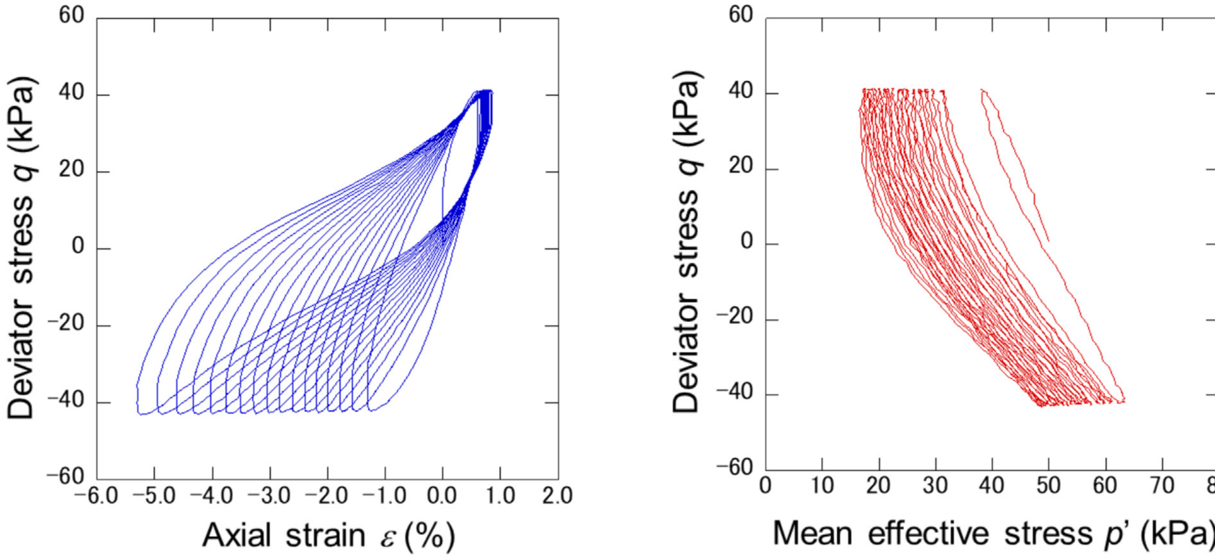

Fig 11. *(continued)*

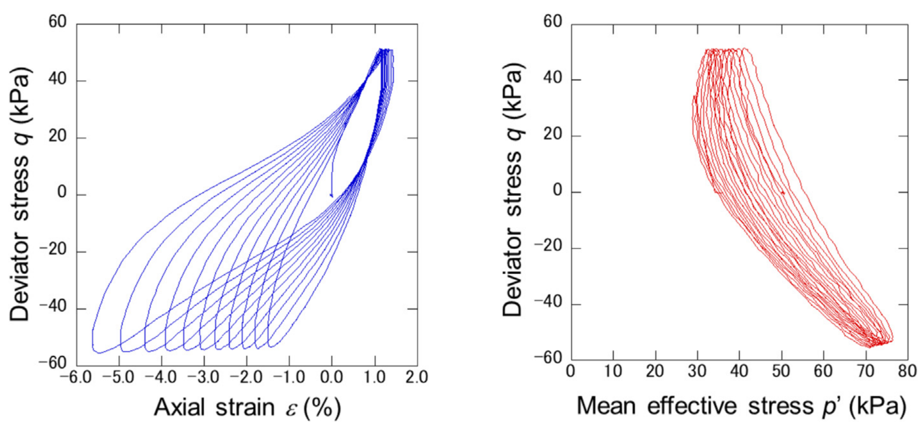

Fig 11. *(continued)*

$$R^* = \frac{p^{*\prime}}{\widetilde{p}'} = \frac{q^*}{\widetilde{q}},\ 0 < R^* \leq 1 \tag{1}$$

$$R = \frac{p'}{\widetilde{p}'} = \frac{q}{\widetilde{q}},\ 0 < R \leq 1, R = \frac{1}{\mathrm{OCR}} \tag{2}$$

where (p', q), $(p^{*\prime}, q^*)$, and $(\widetilde{p}', \widetilde{q})$ represent the present stress state, the corresponding normally consolidated stress state, and the structured stress state on the $p' - q$ plane, respectively. The subloading yield surface is given in the following form:

$$\begin{aligned} & f(p', \eta^*, \zeta) + MD\ln R^* - \mathrm{MD}\ln R - \int_0^t J\mathrm{tr}\boldsymbol{D}^p d\tau \\ &= MD\ln\frac{p'}{p'_0} + MD\ln\frac{\mathrm{M}^2 - \zeta^2 + \eta^{*2}}{\mathrm{M}^2 - \zeta^2} + MD\ln R^* - MD\ln R - \int_0^t J\mathrm{tr}\boldsymbol{D}^p d\tau = 0 \end{aligned} \tag{3}$$

The other variables in Eqs. (1)–(3) are defined as

$$\begin{aligned} \eta^* &= \sqrt{\frac{3}{2}\widehat{\boldsymbol{\eta}} \cdot \widehat{\boldsymbol{\eta}}}, \widehat{\boldsymbol{\eta}} = \boldsymbol{\eta} - \boldsymbol{\beta}, \boldsymbol{\eta} = \frac{\boldsymbol{S}}{p'}, \boldsymbol{S} = \boldsymbol{T}' + p'\boldsymbol{I}, p' \\ &= -\frac{1}{3}\mathrm{tr}\boldsymbol{T}', \zeta = \sqrt{\frac{3}{2}\boldsymbol{\beta} \cdot \boldsymbol{\beta}}, \eta = \sqrt{\frac{3}{2}\boldsymbol{\eta} \cdot \boldsymbol{\eta}} \end{aligned} \tag{4}$$

where $\boldsymbol{S}$ is the deviatoric stress tensor, $\boldsymbol{\beta}$ is the anisotropic stress tensor, and $\boldsymbol{T}'$ is the Cauchy effective stress tensor that is assumed to be positive in tension. J is the Jacobian determination of deformation gradient tensor $\boldsymbol{F}$. D is the dilatancy parameter which can be expressed by $\widetilde{\lambda}$and$\widetilde{\kappa}$, the compression and swelling indices, respectively, as follows:

$$D = \frac{\widetilde{\lambda} - \widetilde{\kappa}}{M(1 + e_0)} \tag{5}$$

$\boldsymbol{D}^p$ denotes the plastic component of stretching $\boldsymbol{D}$, assumed to be positive in tension, and is related to the plastic volumetric strain rate in the following form under the condition

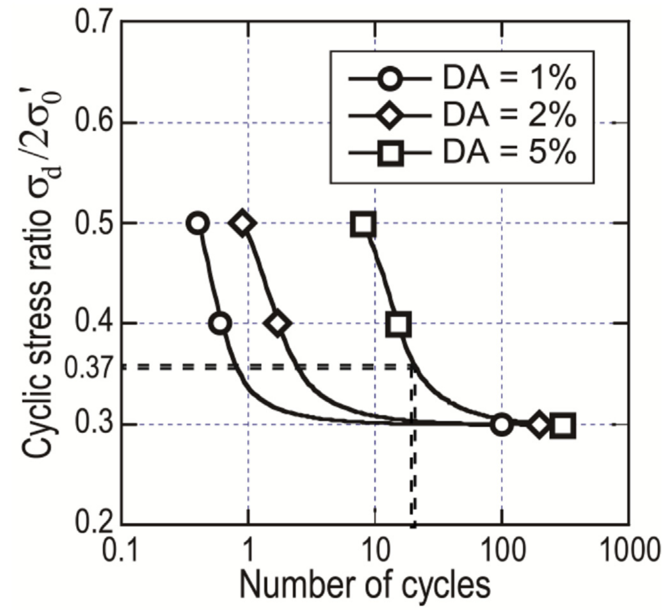

Fig 11. *(continued)*

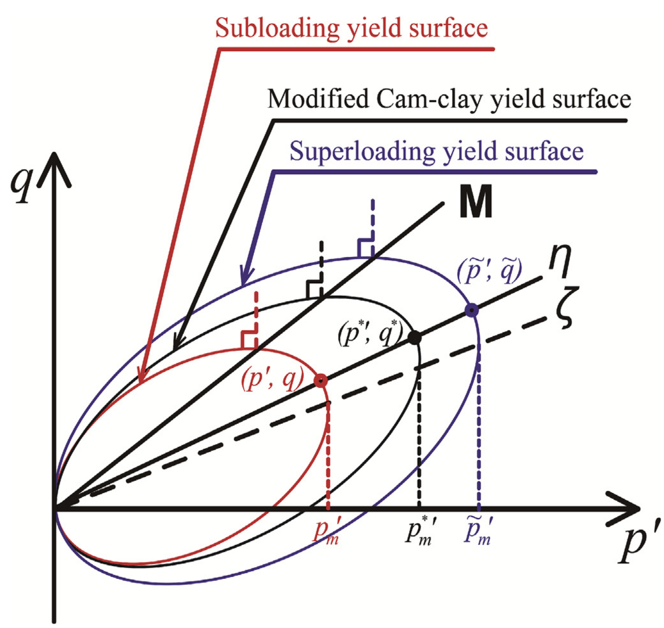

Fig. 12. Yield surfaces of transformation stress-cyclic mobility (TS-CM) model developed by Zhang et al. (2007).

that the compressive volumetric strain is supposed to be positive:

$$\varepsilon_v^p = -\int_0^t J\mathrm{tr}\boldsymbol{D}^p d\tau \tag{6}$$

An associated flow rule is employed in the model, namely,

$$\boldsymbol{D}^p = \lambda\frac{\partial f}{\partial \boldsymbol{T}'} \tag{7}$$

The consistency equation for the subloading yield surface can then be given as

$$\frac{\partial f}{\partial \boldsymbol{T}'}\cdot\dot{\boldsymbol{T}}' + \frac{\partial f}{\partial \boldsymbol{\beta}}\cdot\dot{\boldsymbol{\beta}} + MD\frac{\dot{R}^*}{R^*} - MD\frac{\dot{R}}{R} - J\mathrm{tr}\boldsymbol{D}^p = 0 \tag{8}$$

In the present model, the gradient of the critical state line (C.S.L) is constant and the flat ratio of the elliptical yield surface changes with the value of anisotropy.

The following evolution rule for the anisotropic stress tensor is defined as

$$\dot{\boldsymbol{\beta}} = \lambda\frac{JM\sqrt{6}b_r(b_l\mathrm{M}-\zeta)\hat{\boldsymbol{\eta}}}{\left(M^2-\zeta^2+\eta^{*2}\right)p'} \tag{9}$$

where b_r is an evolution parameter of anisotropy used to control the developing rate of stress-induced anisotropy when the soil is subjected to shearing or compression, b_l is a limitation parameter employed to avoid the singularity in Eq. (3) at point $\zeta = \mathrm{M}$, and 0.95 is used for the value of b_l throughout this paper. In the evolution rule, the stress-induced anisotropic stress tensor will not exceed the C.S.L.

The following evolution rule for degree of structure R^* is defined as

$$\dot{R}^* = J\frac{a}{\mathrm{D}}R^*(1-R^*)\sqrt{\frac{2}{3}}\|\boldsymbol{D}_s^p\| = \lambda\frac{2JMaR^*(1-R^*)\eta^*}{\left(M^2-\zeta^2+\eta^{*2}\right)p'} \tag{10}$$

where $\boldsymbol{D}_s^p$ represents the shear components of the plastic stretching tensor, and a is the degradation parameter of the structure which controls the collapse rate of the structure when the soil is subjected to shearing or compression. It is the same as in the work by Asaoka et al. (2002).

The following evolution rule for degree of overconsolidation R is controlled by the plastic component of stretching and the increment in anisotropy, and defined as

$$\begin{aligned}\dot{R} &= -J\frac{m}{D}\left\{\frac{\left(p'/p'_0\right)^2}{\left(p'/p'_0\right)^2+1}\right\}\ln R\|\boldsymbol{D}^p\| + \frac{R}{MD}\frac{\eta}{M}\frac{\partial f}{\partial\boldsymbol{\beta}}\cdot\dot{\boldsymbol{\beta}} \\ &= \lambda\frac{-mJM\ln R\sqrt{6\eta^{*2}+\frac{1}{3}\left(M^2-\zeta^2\right)^2}}{\left(M^2-\zeta^2+\eta^{*2}\right)p'}\left\{\frac{\left(p'/p'_0\right)^2}{\left(p'/p'_0\right)^2+1}\right\} + \frac{R}{MD}\frac{\eta}{M}\frac{\partial f}{\partial\boldsymbol{\beta}}\cdot\dot{\boldsymbol{\beta}}\end{aligned} \tag{11}$$

where m is the degradation parameter of the overconsolidation state which controls the losing rate of overconsolidation when the soil is subjected to shearing or compression, and p_0' is the reference stress which equals 98 kPa. Its evolution rule was originally proposed by Zhang et al. (2007) and modified by Morikawa et al. (2012).

Nine parameters are included in the present model, among which five, M, e_0, λ, κ, and ν, are the same as those used in the Cam-clay model. The other three parameters are the parameters which control the collapse rate of the structure, the losing rate of over-consolidation, and the developing rate of stress-induced anisotropy. In this paper, those parameters are determined so as to precisely match the aforementioned tri-axial compression tests. Fig. 13(a) and (b) show the performances of the element simulation for the behavior of the clay in undrained static compression tests and oedometer tests on the intact samples taken from the shallow and deep layers, respectively. The values of the material parameters and the initial conditions used in the

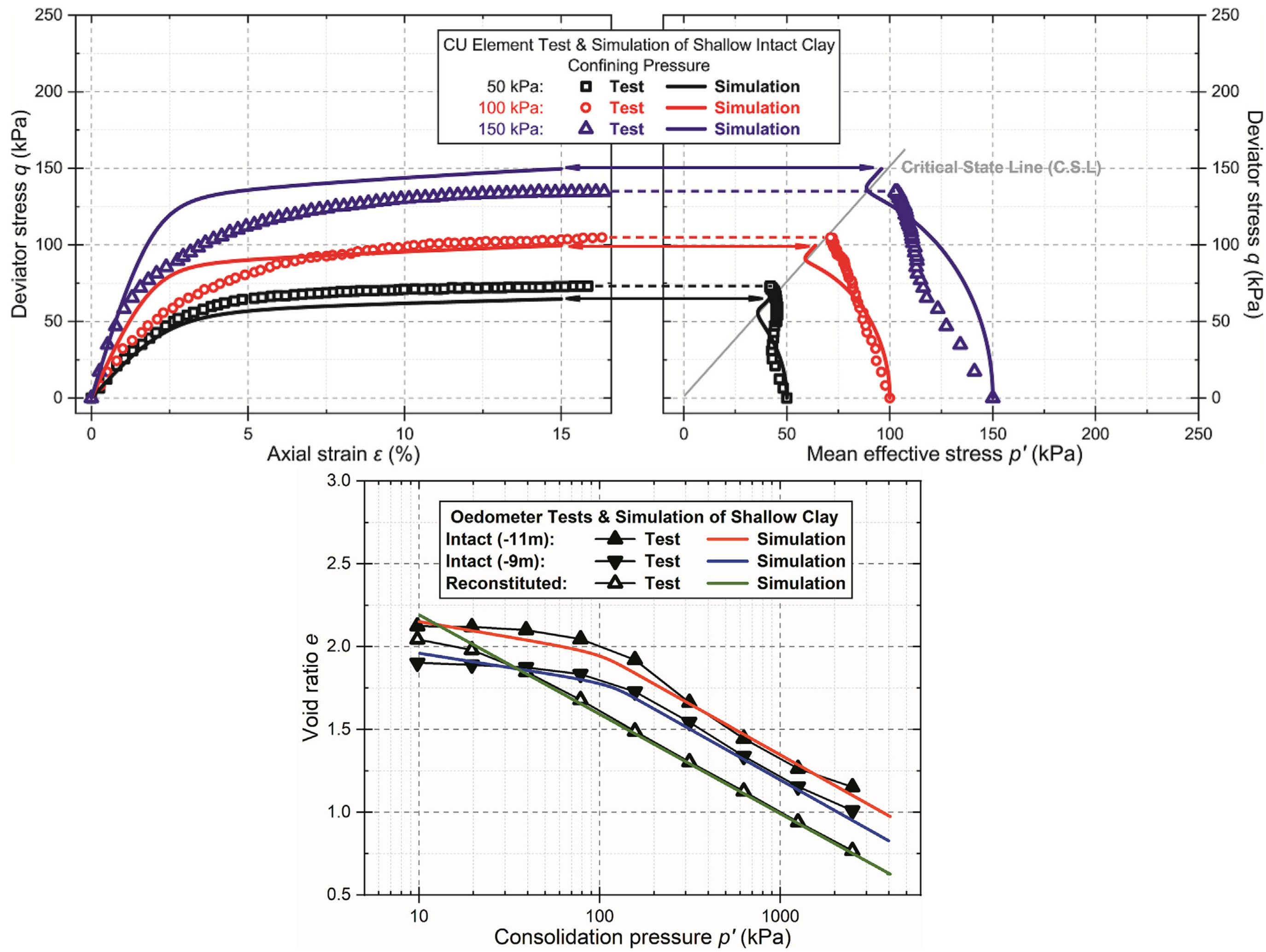

Fig. 13. (a) Simulation results of static CU triaxial compression and oedometer tests on intact samples from shallow layer. (b) Simulation results of static CU triaxial compression and oedometer tests on intact samples from deep layer. (c) Simulation results of static CU triaxial compression tests on samples from silt layer.

simulations are listed in Table 4. It is noted that the R_f given in the table has been converted from M. It can be judged from these figures that the simulation results agree well with the experimental results, except for the case of very high confining pressure. Furthermore, as indicated in Table 4, deep clay structures demonstrate greater susceptibility to degradation, as illustrated by the significantly higher degradation parameter for the deep clay (mR^*) as compared to the shallow clay (0.45 compared to 0.03), despite both types of clay having the same degree of structure ($R_0^* = 0.2$). Fig. 13(c) shows the results of the element simulation for the samples taken from the silt layer. Soil was not sampled from the silt layer in previous field investigations because no subsidence was observed in that layer. In this simulation, the values of the parameters for the silt layer are assumed to be those of typical silt, such as Fujinomori clay. The parameters of Fujinomori clay are taken from Nakai and Hinokio (2004) and Isobe et al. (2014b). The boundary value problem (B.V.P.) is executed using the above parameters to investigate the settlement mechanism after the quake and to predict the amount of subsidence in the future. Fig. 14(a), (b), and (c) present the results of the simulation of cyclic triaxial tests for stress ratios of 0.3, 0.4, and 0.5, respectively. According to these figures, the cyclic undrained behavior could not be reproduced with perfect accuracy, which may have impacted the analytical results to some extent. However, the authors believe that the results are reasonably accurate, except for the situation of SR = 0.3, given that the parameters used here fall within a reasonable range from a physical perspective. The discrepancy between the experimental and analytical results for SR = 0.3 compared to SR = 0.4 or 0.5 is due to a slight underestimation of the initial stiffness in the analytical model under low confining pressure conditions (50 kPa), as shown in Fig. 13(b). This underestimation leads to an overestimation of double amplitude (DA) axial strain when cyclic shear is applied under the same low confining pressure. The effect is particularly pronounced for SR = 0.3, causing the results to deviate more significantly from the experimental data. Fig. 14(d) presents liquefaction strength curves and

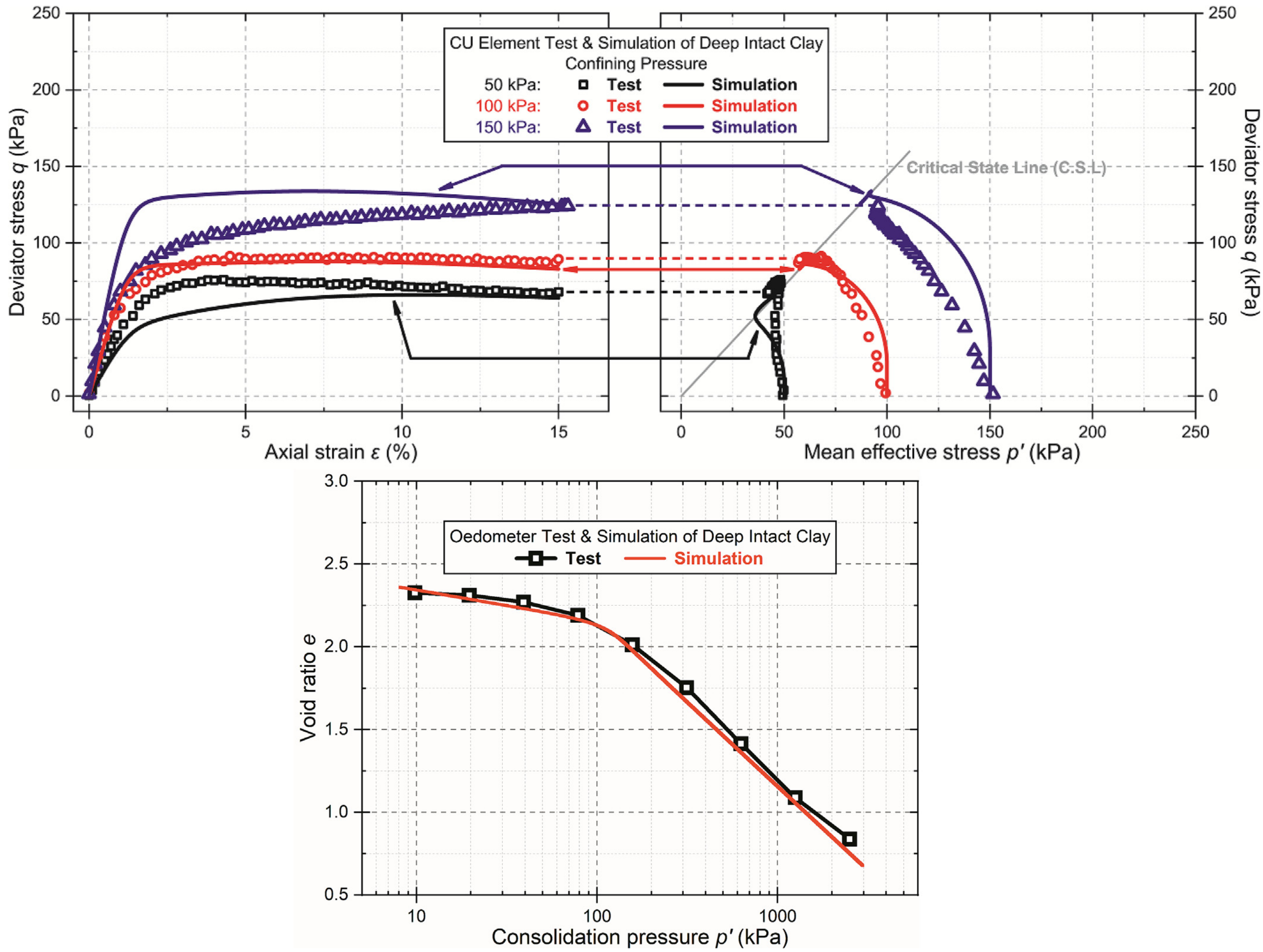

Fig 13. *(continued)*

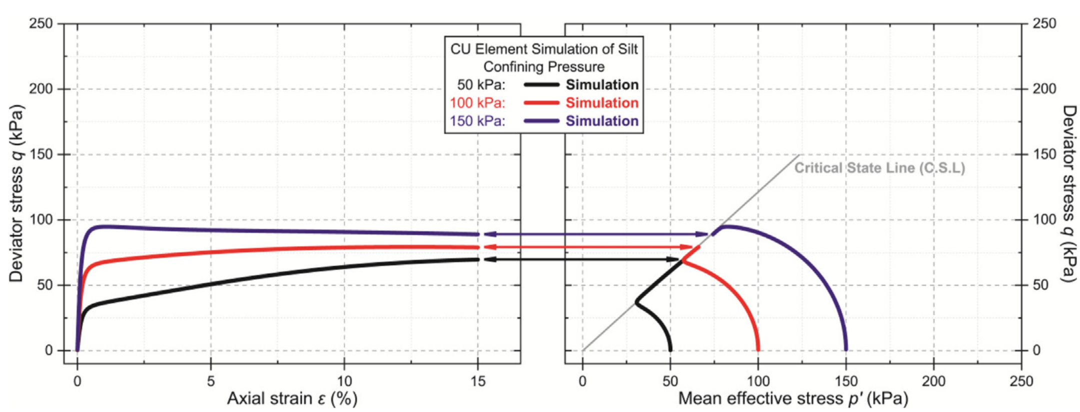

Fig 13. *(continued)*

the excess pore water pressure (EPWP) at DA = 5 % for the deep layer obtained by the cyclic triaxial tests and simulation. By referring to this figure and examining the EPWP caused by cyclic shear, only a minimal discrepancy is found between the experimental and analytical results. Since the increase in EPWP is thought to be the primary cause of the long-term settlement in soft clay after an earthquake, and an element simulation is able to reasonably evaluate this increase, the analytical parameters used in this study are considered appropriate and reliable.

Table 4
Soil parameters used in simulation.

		Shallow layer	Deep layer	Silt	Gravel
Compression index	λ	0.266	0.440	0.104	
Swelling index	κ	0.050	0.031	0.010	
Stress ratio at critical state $R_f = (2*\boldsymbol{M} + 3) / (3-\boldsymbol{M})$	R_f	4.200	3.800	3.800	
Void ratio ($p' = 98$ kPa on N.C.L)	N	1.617	1.548	0.920	0.600
Maximum historical preconsolidation pressure	p'_c	70.0	80.0	120.0	
Poisson's ratio	v	0.370		0.200	0.300
Degradation parameter of overconsolidation state	mR	25.0		2.2	
Degradation parameter of structure	mR^*	0.030	0.450	0.100	
Evolution parameter of anisotropy	br	0.10	0.70	0.10	
Initial mean effective stress [kPa]	p'	8 ~ 73	78 ~ 111	117 ~ 295	
Initial degree of structure	R_0^*	0.20	0.20	0.10	
Initial degree of overconsolidation − OCR	$1/R_0$	1.3 ~ 10.5	1 ~ 1.4	2.5	
Initial anisotropy	ζ_0	0.0	0.2	0.0	
Permeability [m/sec]	k	7.0×10^{-10}		1.0 x 10^{-10}	1.0 x 10^{-4}
Saturated unit weight [kN/m^3]	γ_{sat}	15.36	15.66	17.00	19.00
Unit weight under water [kN/m^3]	γ'	5.36	5.66	7.00	9.00
Young's modulus [GPa]	E				100.0

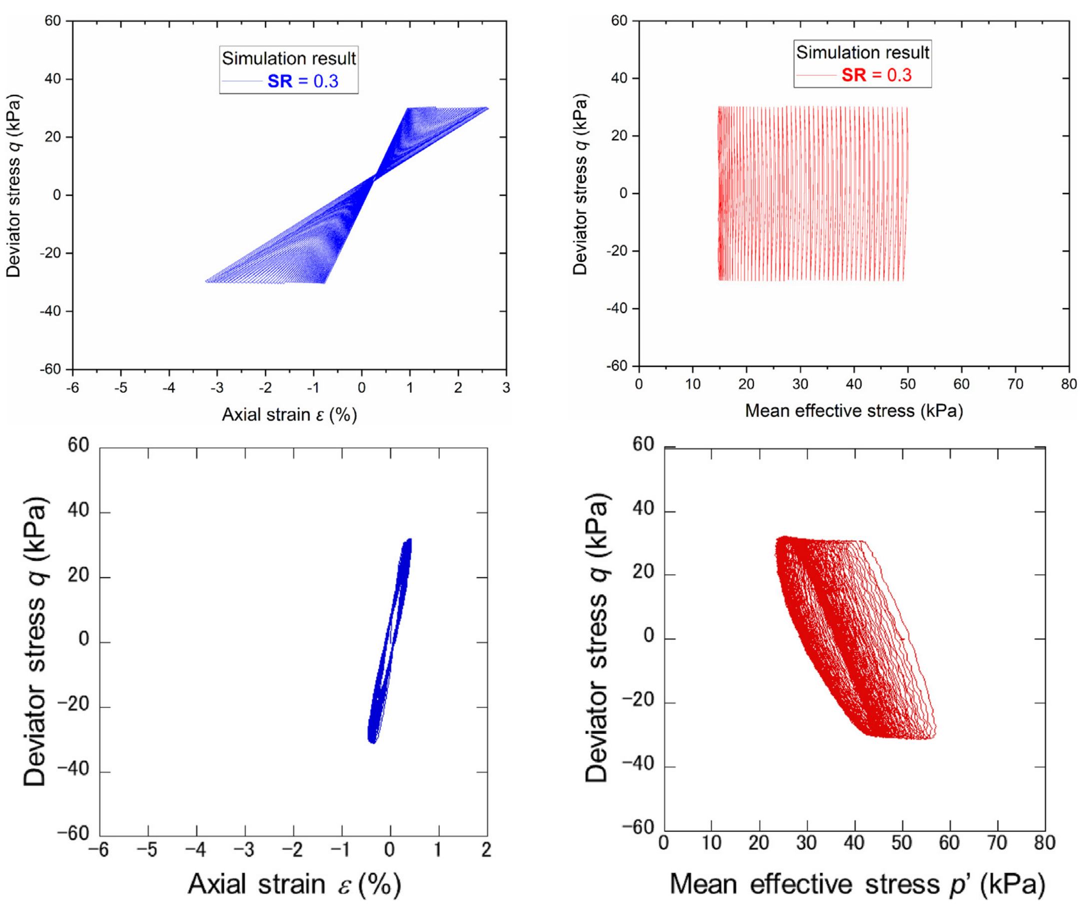

Fig. 14. (a) Results of simulation of cyclic triaxial tests (σ_d / $2\sigma_0' = 0.3$). (b) Results of simulation of cyclic triaxial tests (σ_d / $2\sigma_0' = 0.4$). (c) Results of simulation of cyclic triaxial tests (s_d / 2 $s_0' = 0.5$). (d) Liquefaction strength curves and excess pore water pressure (EPWP) at DA = 5 % of deep layer obtained by cyclic triaxial tests and simulation.

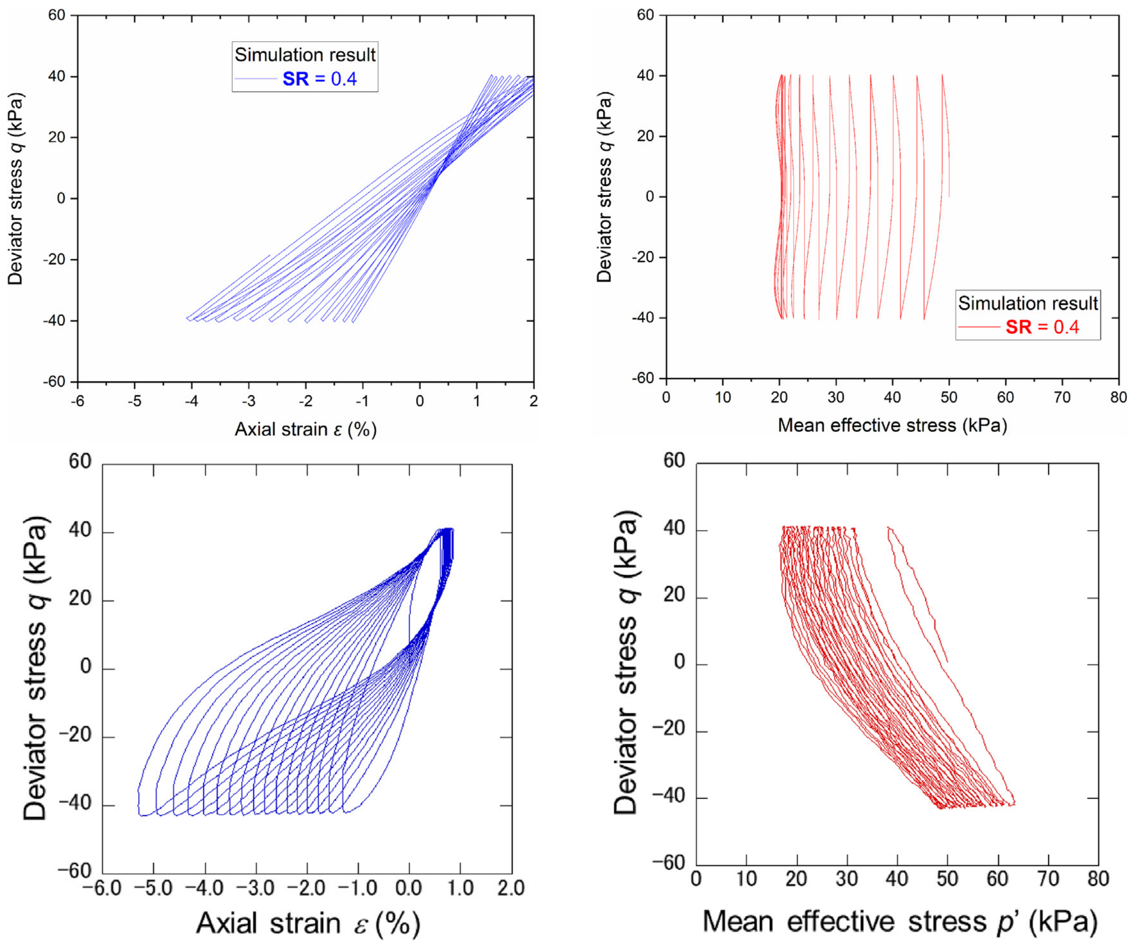

Fig 14. *(continued)*

4.2. Analytical conditions

The soil–water coupling FE analysis code DBLEAVES (Ye et al., 2007) is used in the simulation. This 2D and 3D FE analysis program is able to solve the repeated static and dynamic soil–water coupled B.V.P. by using Oka's two-phase field theory (Oka et al., 1992, 1999) and the FE-FD soil–water coupled method. The FE model is simplified to a one-dimensional column of soil elements, whose size is 1 m in width, 1 m in length, and 1 m in height, as shown in Fig. 15. Here it is assumed that the ground is level and the effects of the terrain geometrics are not considered in the simulation. The ground water level is assumed at GL −1.0 m as it is slightly lower than the ground surface according to on-site observation data. The EPWP is not calculated in the surface element (#50) above the groundwater level. The boundary conditions are that: (a) the bottom of the ground is a viscous boundary (Lysmer and Kuhlemeyer, 1969), (b) in the dynamic analysis, an equal-displacement-boundary condition (Yashima et al., 1991) is used between the nodes on two sides of the ground and, when the analysis is shifted to consolidation, the boundary condition is then changed to a fixed one, and (c) a depth of 1 m is set as the drainage condition, while the other surfaces are impermeable. The V_p and V_s values used for the viscous boundary were estimated from the P, S velocities in the K-NET (Station No. NIG018 near "City Hall" or "A" in Fig. 5) provided in the reference (Strong-motion Seismograph Networks (K-NET, KiK-net)) shown in Fig. 7, with V_s and V_p determined as 500 m/s and 1500 m/s, respectively.

In the numerical simulation, the process during shaking is simulated by a dynamic soil–water coupled analysis, while the process of the dissipation of EPWP is simulated by a static consolidation analysis. The whole process is a continuous one; and therefore, it should be continuously simulated sequentially. The simulation is divided into the following two stages: (a) the dynamic analysis lasting 280 s until the shaking stops and (b) the consolidation analysis lasting 150 years until the EPWP dissipates completely. The initial stress field is calculated by a self-weight static analysis in advance, and the values for the unit weight and range in initial stress for each layer are shown in Table 4. The value of the initial over-consolidation ratio (OCR) in the analysis is calculated automatically by the DBLEAVES analysis code using the maximum historical pre-consolidation pressure of 70 kPa for the shallow layer and 80 kPa for the deep layer, as given in Table 4.

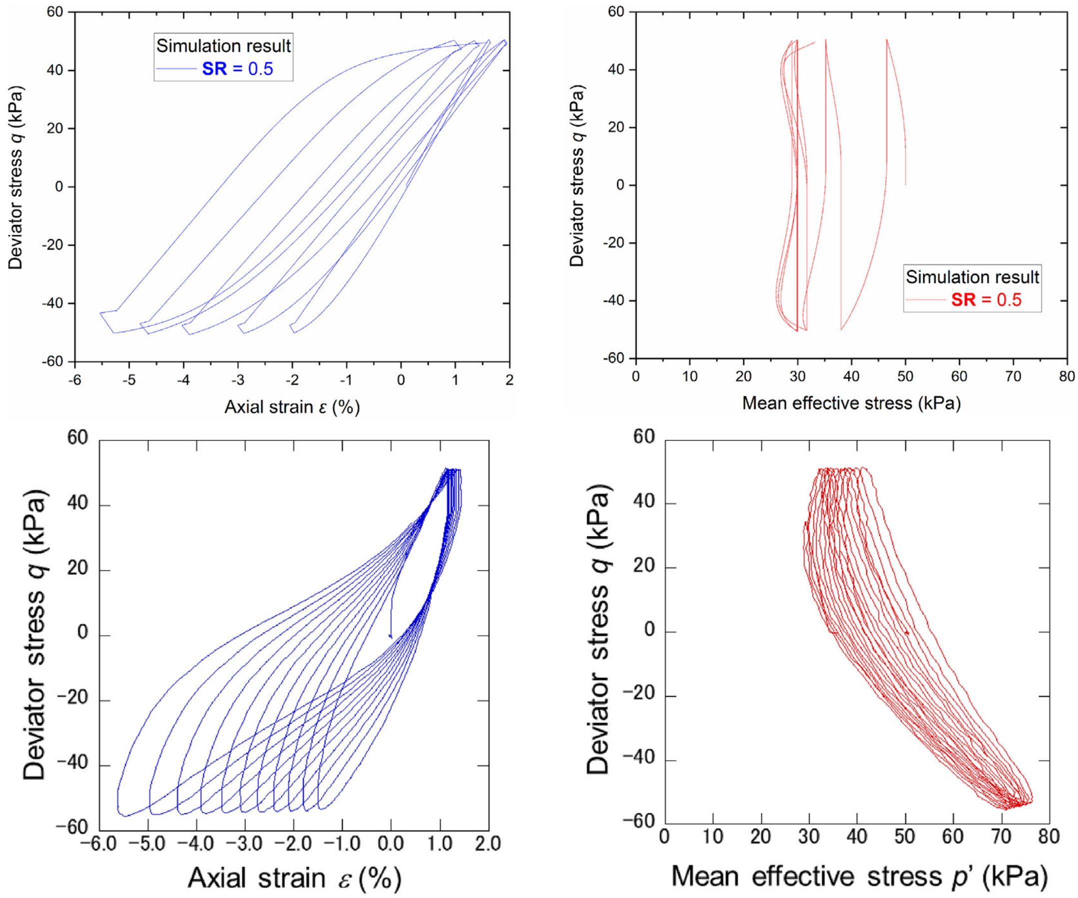

Fig 14. *(continued)*

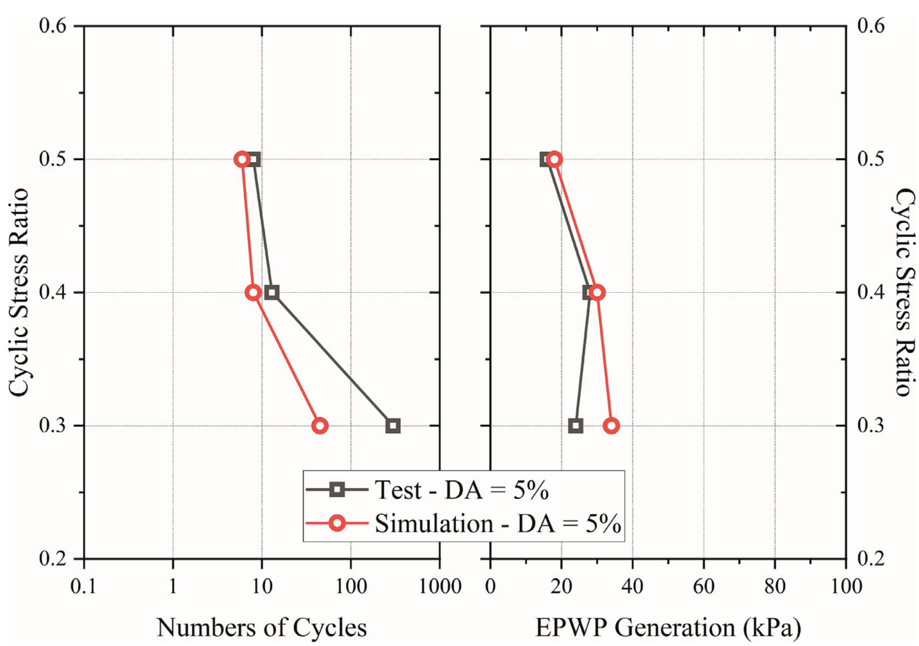

Fig 14. *(continued)*

The input motion on the base layer of the objective site in the Niigata-ken Chuetsu-oki Earthquake of 2007 was estimated in two steps. Firstly, the peak acceleration at two sites of the KiK-net observation station (Kawanishi

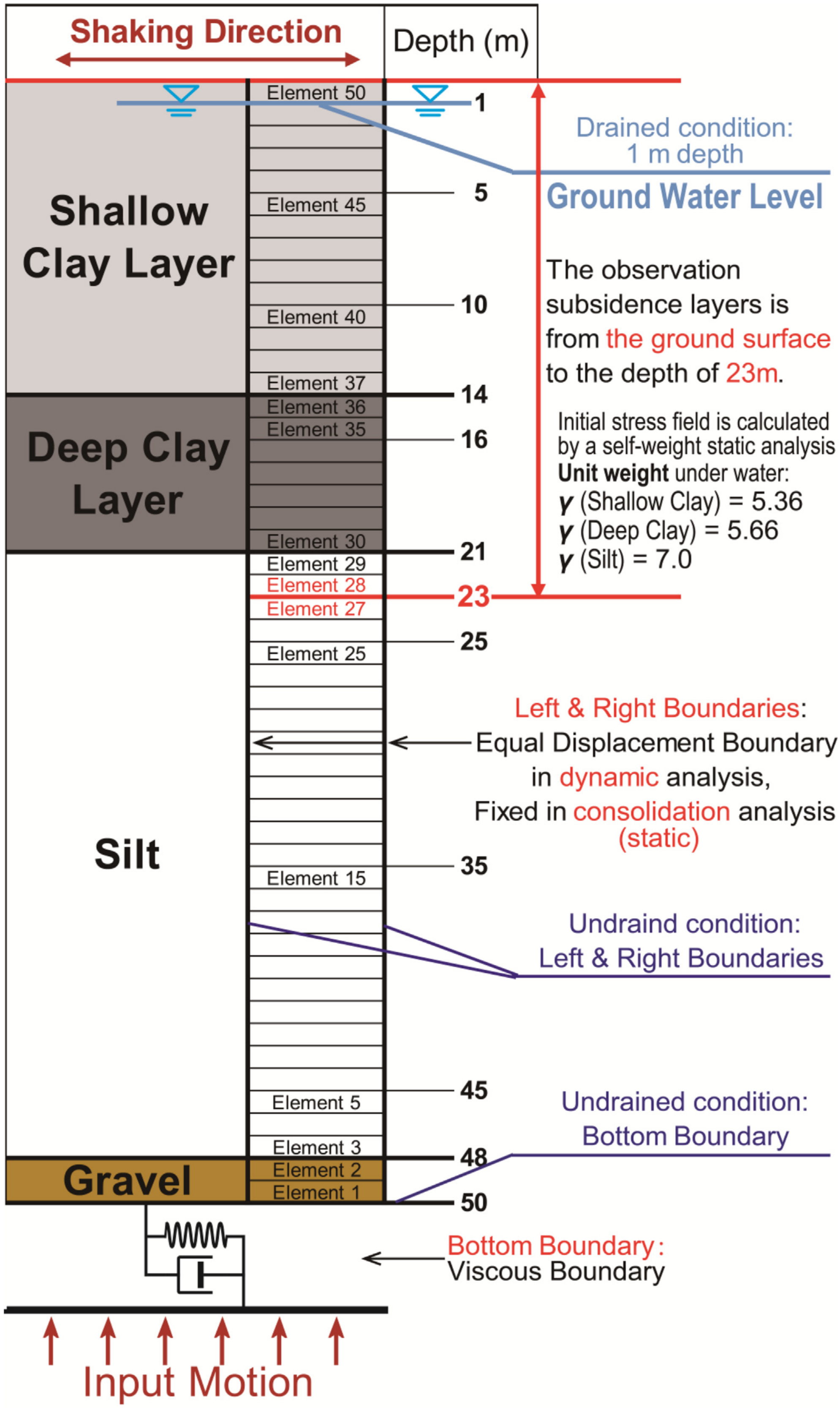

Fig. 15. Finite element mesh and boundary conditions used in simulation.

Station and Yunotani Station) were predicted by the Si-Midorikawa attenuation relationship (1999). Secondly, the base acceleration waves for both sites were back analyzed from the observed acceleration waves on the surface using a one-dimensional elastic model with multiple layers. In the calculation, the soil parameters were determined from laboratory tests and PS loggings, except for the damping ratio. The damping ratio was specified so as to express the observed base waves. The calculated base waves were then separated into ascending and descending waves to compare them with the estimated peak acceleration. As the estimated peak acceleration had the trend of overestimation, the estimated peak accelerations were reduced to 0.7 times. Ultimately, the peak acceleration on the free surface of the engineering foundation in Kashiwazaki City was estimated as 96 Gal, and the proportionated acceleration wave on the base layer at Yunotani was adopted as the input wave.

Fig. 16 shows the time history of the input acceleration used in the simulation, applied at the bottom of the analytical domain. Stiffness proportional damping, with a damping rate of 5 %, was applied for the damping model, and the Newmark-β method ($\beta = 0.3025$ and $\gamma = 0.6$) was used for the time integration.

4.3. Comparison of simulation and observation

Fig. 17 shows the time history of the response acceleration on the ground surface and the input acceleration, while Fig. 18 shows a comparison of the time histories of the cumulated ground subsidence of the soil layers to a depth of 23 m between the observation and the FE analysis results. It is obvious from Fig. 17 that the response acceleration on the ground surface was 116 Gal, and that the small amount of shaking on the ground surface lasted 160 sec. The results of the subsidence observation included not only the settlement caused by the earthquake and consolidation, but also the settlement caused by autumn and winter pumping. Therefore, the results of the settlement simulation for the earthquake and consolidation should be slightly smaller than the subsidence observation which included the former. The ground subsidence given in Fig. 18 started to gradually increase soon after the shaking, having a good and reasonable agreement with the observation results, and lasted for 150 years. The cumulated subsidence, which finally reached 200 mm, was caused by the generation of EPWP in the shallow and deep clayey layers induced by the shaking, and its dissipation took a long period of time because of low permeability. It should be noted that, at the beginning stage, the results of the simulated settlement were a little smaller than the subsidence observation; that is, the settlement calculation for the first month was 3 mm, while the subsidence observation data for the first month was about 8 mm. One possible reason for this difference is that the observed settlement included immediate subsidence, in addition to the consolidation phenomenon, or other factors such as the difference in drained conditions between the actual conditions and the simulated conditions (one-dimensional analysis in the calculation) and other unknown information.

Figs. 19 and 20 present the time histories of the excess pore water pressure ratios (EPWPR) and vertical strain at the different specific depths given in Fig. 15, respectively. It is shown in Fig. 19 that the deeper the soil layer, the

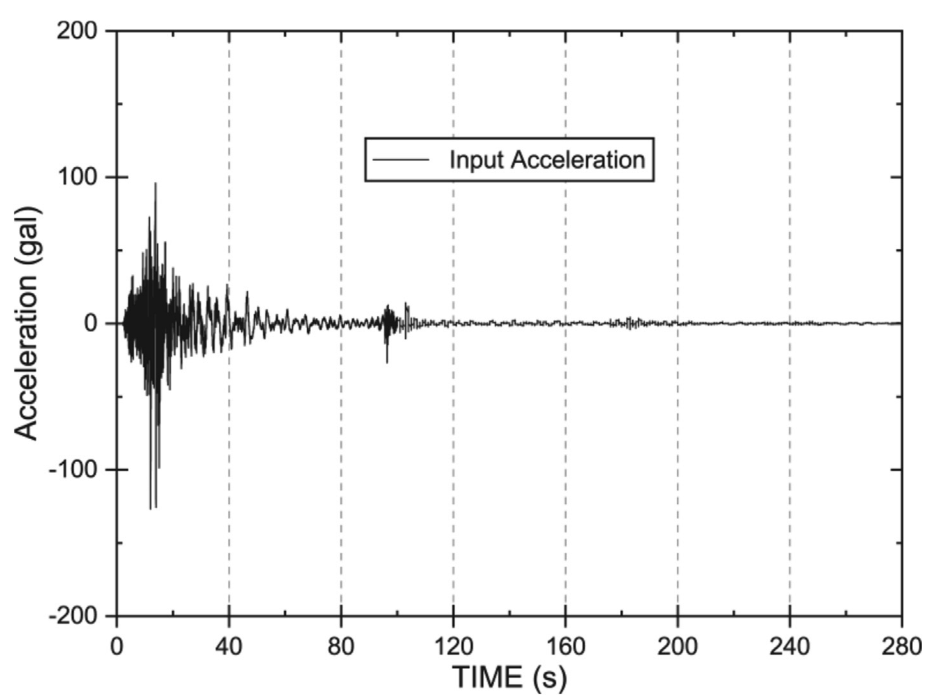

Fig. 16. Time history of input acceleration used in simulation.

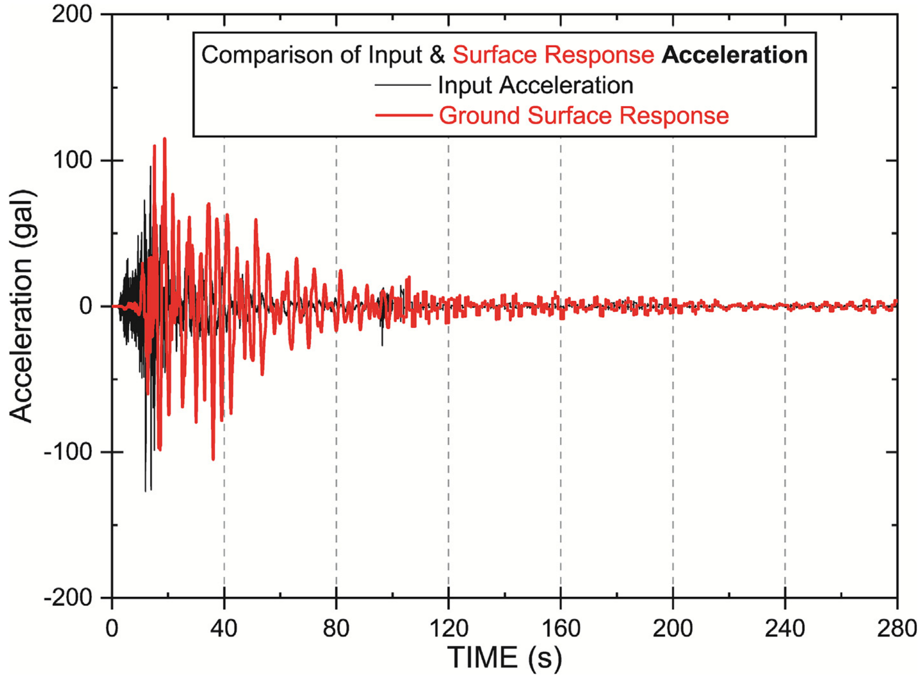

Fig. 17. Time history of response acceleration on ground surface and input acceleration.

smaller the EPWPR after shaking, but the difference in the EPWPRs between the shallow clay and the deep clay is not significant. Additionally, the EPWPR of the shallow clay, which lays close to the ground surface, reached the maximum value of 0.31. It can be analyzed from these results that the reasons for the relatively large post-earthquake subsidence in the Kashiwazaki area covered with soft clay are the generation of excess pore water pressure in the clayey layers, due to the 2007 earthquake, and its slow dissipation. In Fig. 20, the “All 23 m FE Analysis Result” represents the vertical strain of all the clay layers, including the shallow and deep clay layers, with a total thickness of 23 m. It should be noted that, in Fig. 20, the vertical strain in the deep clay layer (depths of 15 m and 20 m represented by the solid and dashed red lines, respectively) is larger than that in the shallow clay layer (depths of 5 m and 10 m represented by the solid and dashed black lines, respectively), which verified the conclusion given in 3.1 that deep clay has more potential to consolidate than shallow clay.

Figs. 21 and 22 show the contour and isochronous curves of the EPWP or EPWPRs distributed in the analytical domain at specific times (initial, during shaking, soon after shaking, 1, 10, 20, and 30 years later). It can be seen from Fig. 21 that the horizontal shaking of the soil during the 280 s of earthquake shaking was not small, while the subsidence was small, but there was a relatively large settlement after the earthquake. In addition, it should be noted that the displacement was magnified 10 times in the figure to facilitate readers to feel the deformation. In Fig. 22, the high EPWPRs for the deep clay and shallow clay are seen in the calculation results. The EPWPRs gradually decrease with the passage of time after the earthquake. There is a distinctive feature or depression at the boundary separating the shallow and deep clay layers, owing to the notable disparity in the capacity of the deep clay and shallow clay to generate EPWP. Following the earthquake, it becomes evident that the EPWPR at this boundary increases abruptly, indicated by the black curve rising to meet the red curve at a depth of 14 m. This suggests that following the earthquake, before being discharged from the drainage boundary, the EPWP and pore water initially propagate and infiltrate from the two peaks of the EPWPR in both the shallow and deep clay layers towards the depression, which serves as the boundary between these layers. Consequently, there is a flattening of the EPWPR curve (transitioning from the black curve to the red one), with the peak of the deep clay layer notably decreasing from post-earthquake to one year later. The dissipation of the EPWPR gradually progresses from the drainage boundary in subsequent years.

Fig. 23 shows the values of C_d (compression index induced by dynamic loading) and vertical strain e obtained by the FE analysis at the different depths of the shallow and deep layers during consolidation after the earthquake. As mentioned in the Introduction, C_d is the ratio of void ratio change Δe during the consolidation process to the comparison of the logarithm values for effective stress before and after excess pore water pressure dissipation caused by dynamic loads. It applies to the relationship $C_s < C_d < C_c$ for both the shallow and deep clay layers. $C_d^{Shallow}$ is approximately in the range of 0.176 to 0.255, while C_d^{Deep} is approximately in the range of 0.230 to 0.381. It is also clear that the C_d of each layer is not constant along depth and has obviously been affected by the OCR in the same

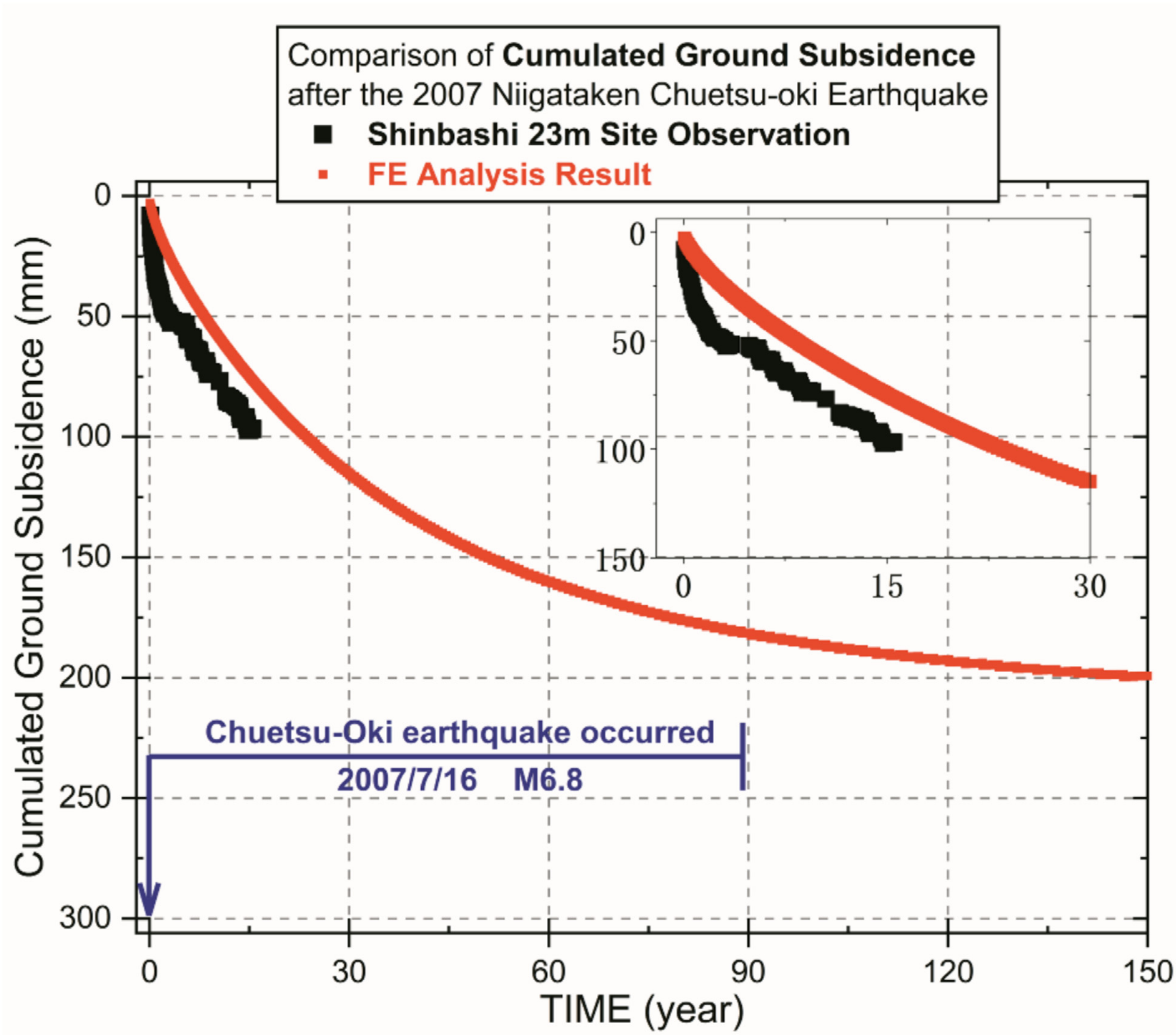

Fig. 18. Comparison of time histories between observation and FE analysis for cumulated ground subsidence of soil layers to depth of 23 *m*.

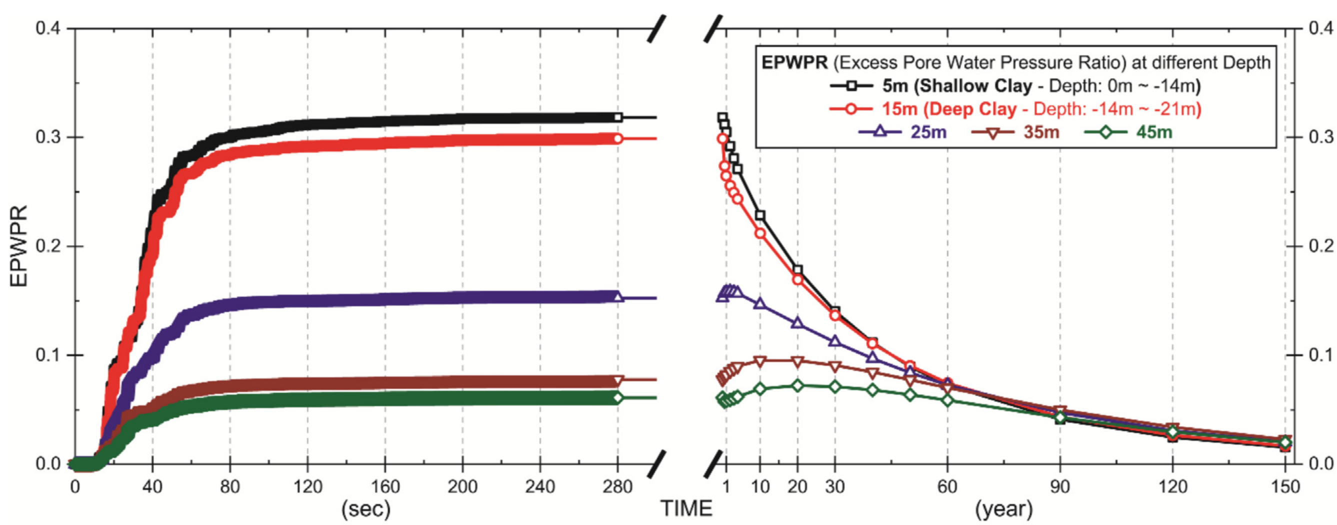

Fig. 19. Time history of excess pore water pressure ratios (EPWPR) at different depths.

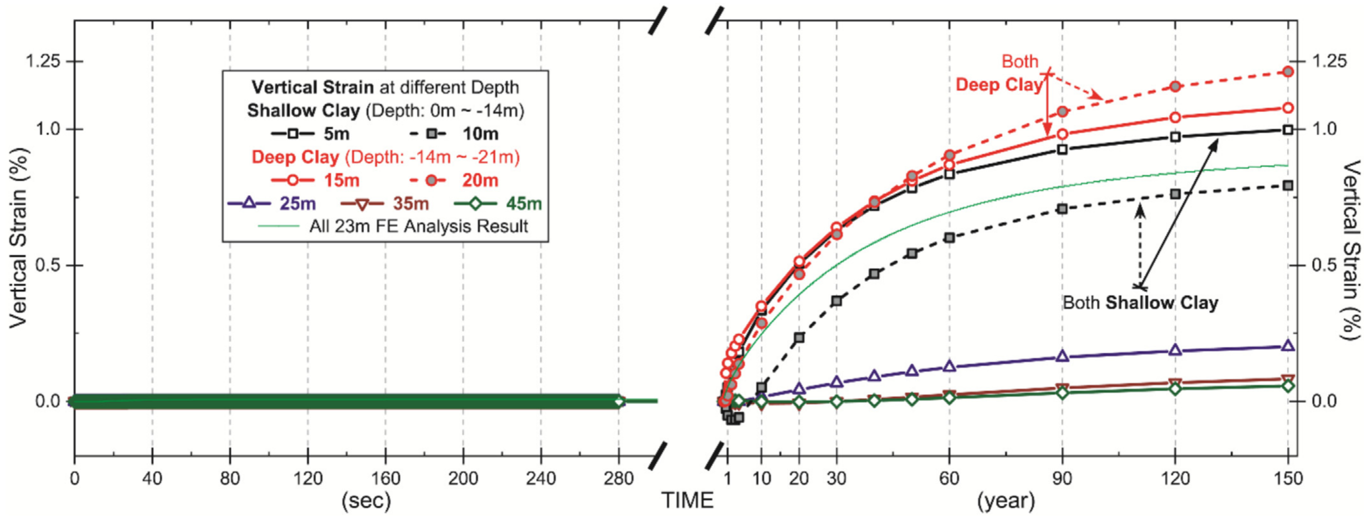

Fig. 20. Time history of vertical strain at different depths.

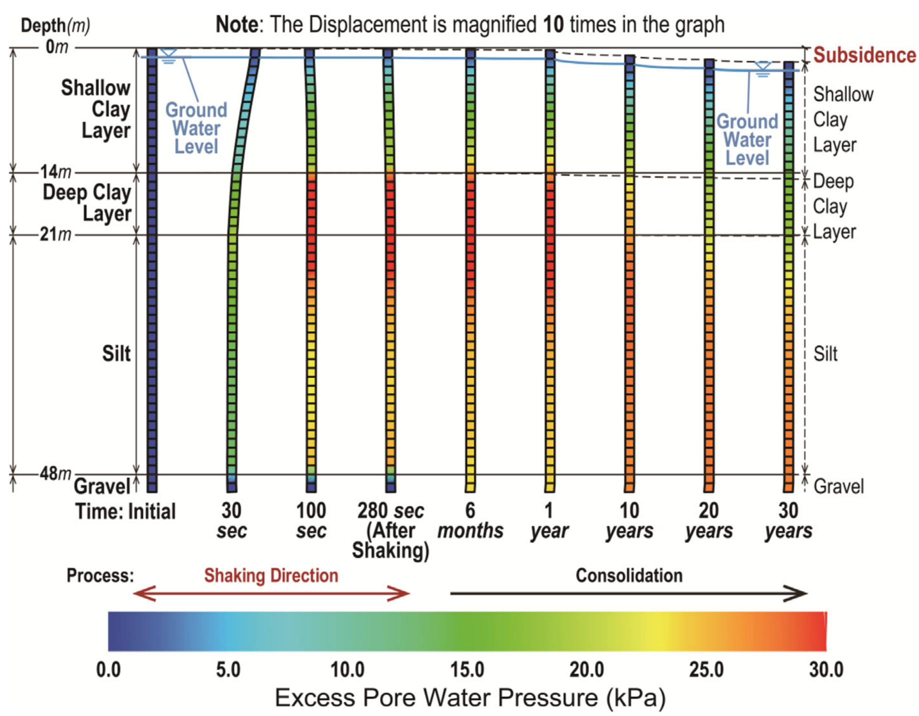

Fig. 21. Contour of excess pore water pressure during and after shaking (The displacement is magnified 10 times in the figure.).

layer of soil, that is, parameter R. The OCR gradually increases as the depth becomes shallower in the same soil layer, while C_d decreases slightly. This phenomenon is consistent with the conclusion of Ohara and Matsuda (1988): "C_{dyn} reduces a little with increase of OCR". Specifically, in the tests of Ohara and Matsuda (1988), C_{dyn} decreased by approximately 26 % as the OCR increased from 1 to 6, while $C_d^{Shallow}$ decreased by about 30 % as the OCR increased from 1 to 9.3 in this study. It can be roughly considered that $C_d^{Shallow} < C_d^{Deep}$, while vertical strain e of the deep layer is also greater than that of the shallow one, which again verifies the conclusions in 3.1 and 4.1, namely, that deep clay has more potential to consolidate and that the structure of deep clay is more susceptible to degradation than shallow clay as the degradation parameter of structure mR^* of deep clay is obviously higher than that of shallow clay (0.45 compared to 0.03).

Although the generation of EPWP in the silt layer was also observed, the cumulated ground subsidence was less than that of the clayey layer because the values of its compression and swelling indices and degradation parameter for the over-consolidation state were small compared to those of the clayey layer. This was based on the time histories of over-consolidation state R and degree of structure

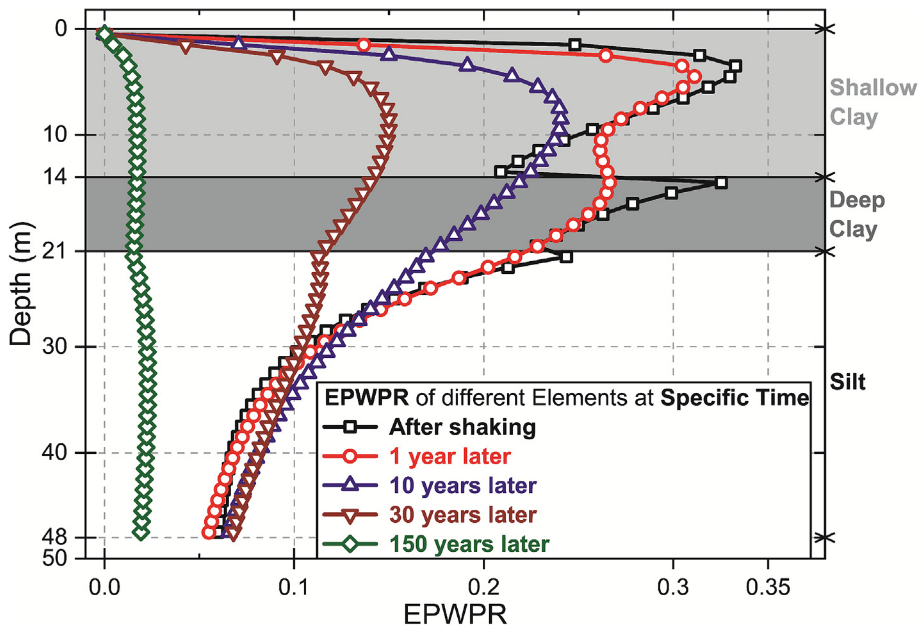

Fig. 22. Isochronous curve of excess pore water pressure ratio for each element.

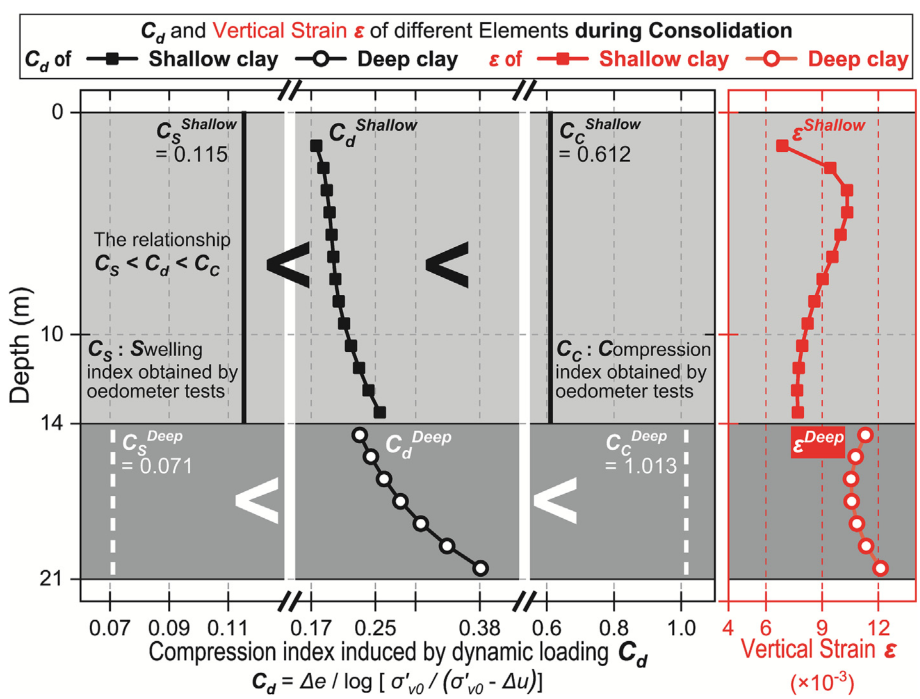

Fig. 23. Values of C_d (compression index induced by dynamic loading) and vertical strain ε obtained by FE analysis at different depths of shallow and deep layers during consolidation after earthquake.

state R^* shown in Fig. 24. It is obvious from the figure that the values for R in all layers decreased due to the generation of EPWP during the shaking and that the values recovered during the dissipation of EPWP. The decrease was especially obvious in the clayey layer, while the R at a depth of 5 m in the shallow clay layer decreased about 0.14 and the R at a depth of 15 m in the deep clay layer decreased about 0.23. This foregoing behavior depended on the value of the parameter of degradation of overconsolidation state mR. In addition, the degrees of structure R^* in the clay layer increased during and after the shaking, implying that the collapse of the natural structure in the clay layer occurred not only under cyclic shearing loading, but also during consolidation. The soil structure degraded during the consolidation process and, as pointed out by Kaneda et al. (2003), it is thought that it took a long

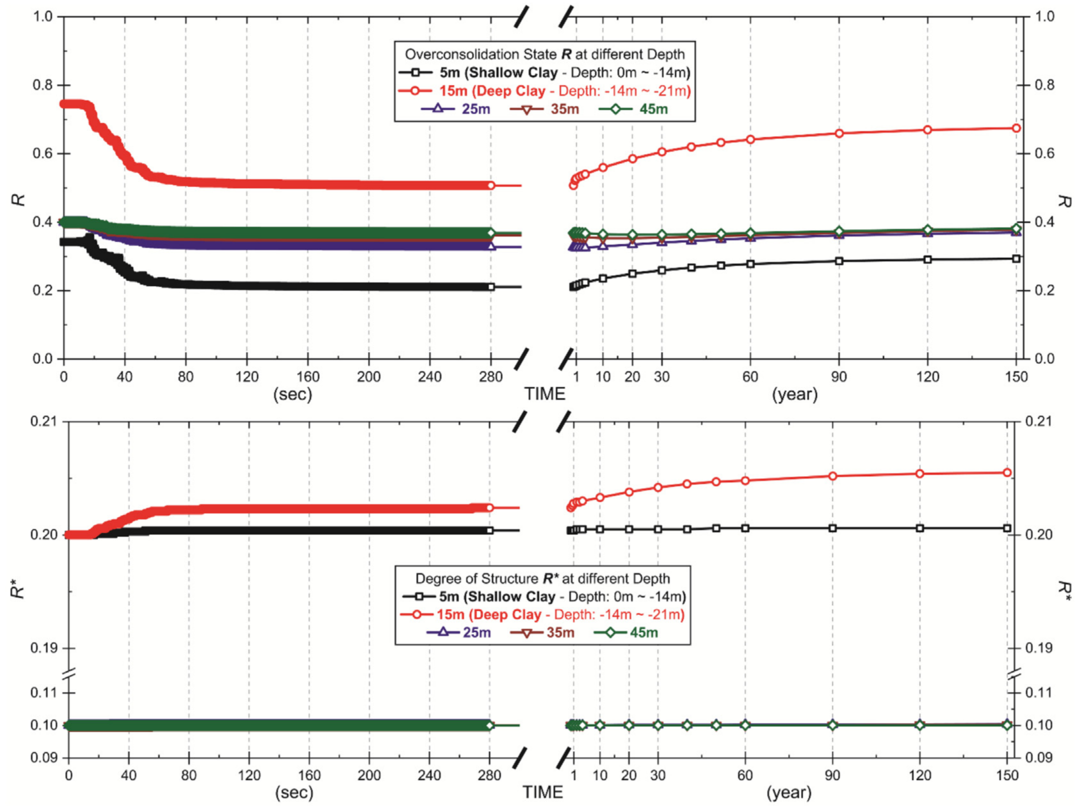

Fig. 24. Time histories of R and R^* at different depths.

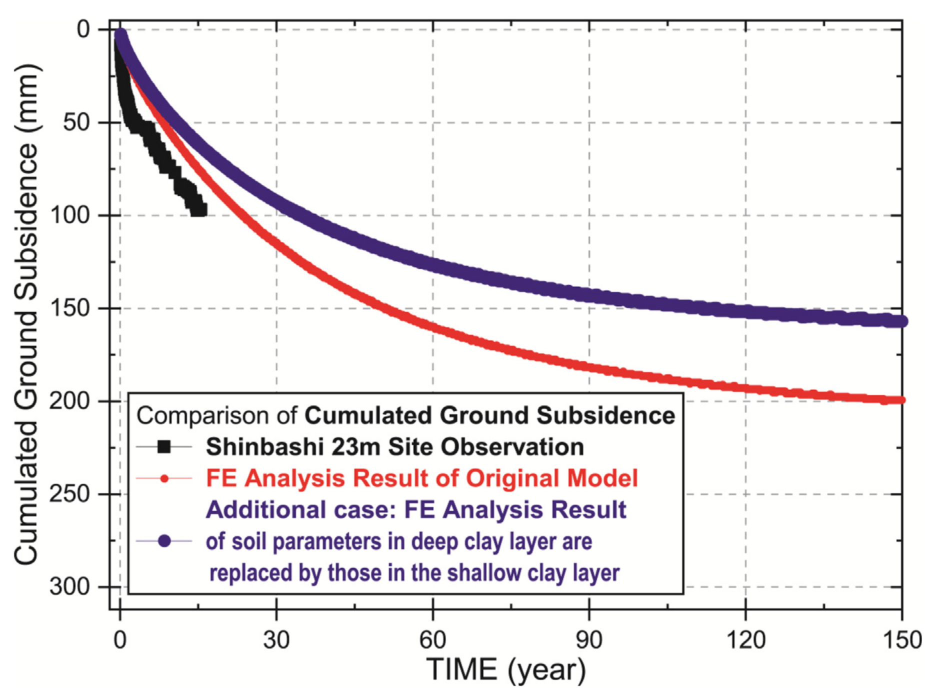

Fig. 25. Comparison of time histories among observation, original FE analysis, and additional simulation case results for cumulated ground subsidence of soil layers to depth of 23 *m*.

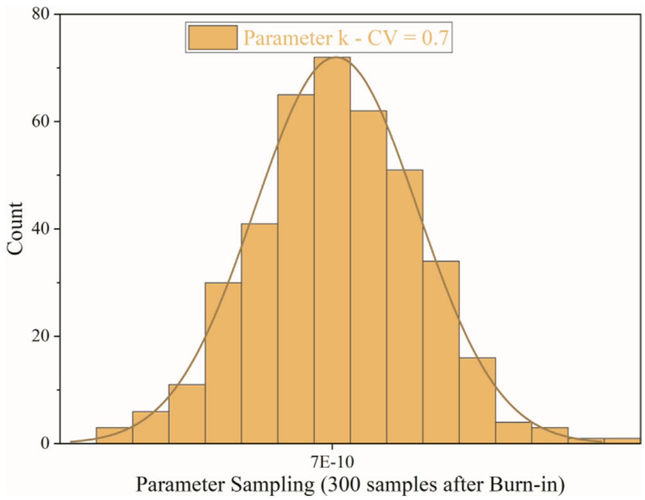

Fig. 26. (a) Input distribution of parameter k 's uncertainty analysis (CV = 0.7). (b) Output of parameter k 's uncertainty analysis (CV = 0.7).

period of time for the EPWP of the structured clay to dissipate. Another difference that should be noted in Fig. 24 is that the increase in R^* in the deep clay layer (depth of 15 m on the red line) is larger than that in the shallow clay layer (depth of 5 m on the black line), which once again verifies the conclusion that deep clay has a greater potential to consolidate than shallow clay.

Subsequently, one numerical experiment was conducted in order to investigate the difference in the shallow and deep clay layers. In this additional case, the soil parameters in the deep clay layer were replaced by those in the shallow clay layer. Fig. 25 presents a comparison of the time histories among the observation, original FE analysis, and additional simulation case on the cumulated ground subsidence of the soil layers to a depth of 23 m. It is obvious from this figure that the ground subsidence will decrease significantly if the parameters of the deep clay layers are all replaced by those of the shallow clay layers. This once again enhances the conclusion that deep clay has more potential to consolidate than shallow clay and that the structure of deep clay is more susceptible to damage than shallow clay. In addition to the degradation parameter of the structure, the difference in shear strain induced by ground motion is also behind the difference in the amount of settlement.

Finally, considering the influence of parameter permeability k on the results, the Monte-Carlo method with the burn-in process was used to analyze the uncertainty of permeability k for deep and shallow soils. "Burn-in" is an informal term used to describe the process of "warming up" at the start of a Monte Carlo (MC) simulation. This

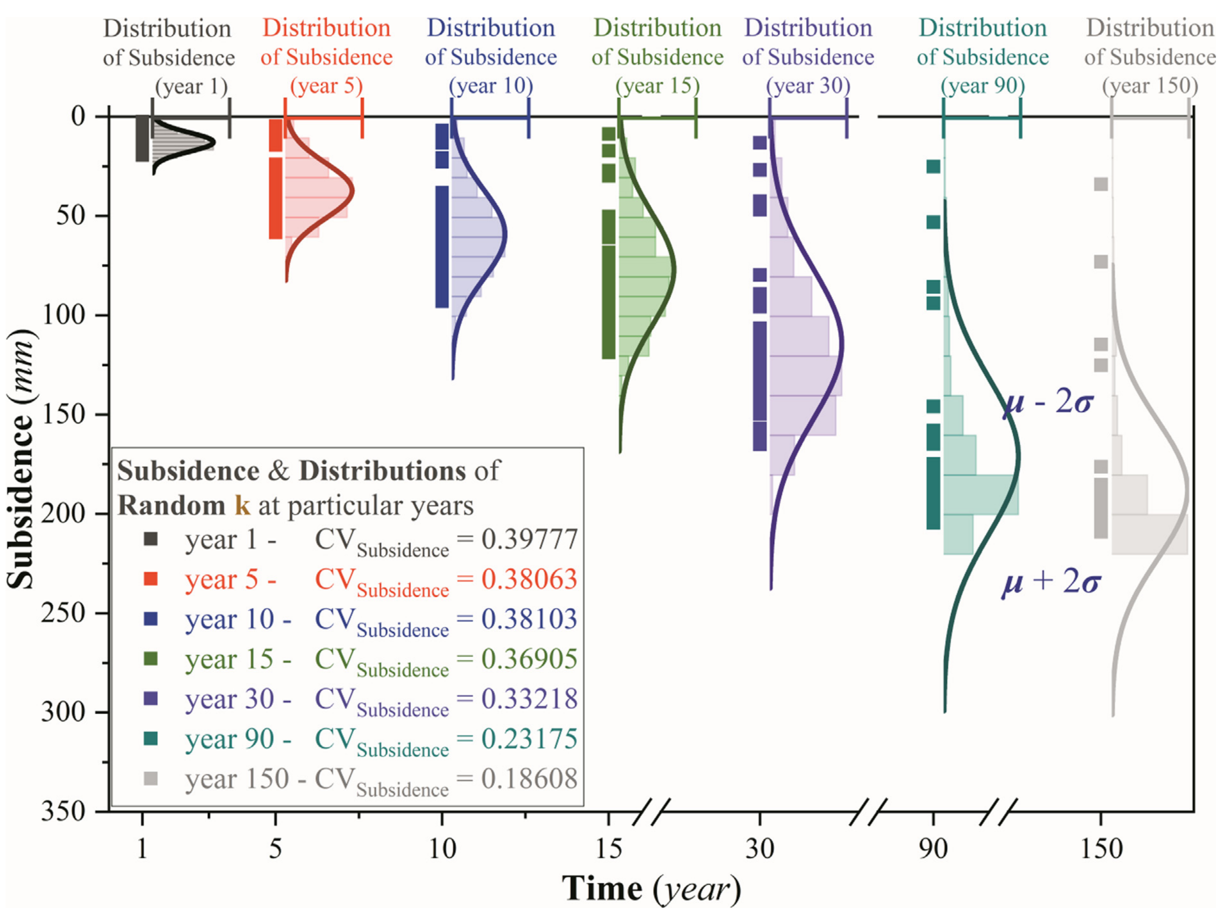

Fig 26. *(continued)*

involves discarding the initial, unstable samples to ensure that the system will reach a stable state before beginning the formal sampling. The decision on when to discard these early samples is usually based on adaptive iterations, which are assessed when the system has stabilized. The analytical method and approach to "burn-in" were detailed in Jiang et al. (2024). An uncertainty analysis was conducted using a custom-built, non-intrusive geotechnical stochastic finite element software called "JRiver_uncertainty," which features a graphical user interface and utilizes parallel computing. The input and output results of parameter k's uncertainly analysis are shown in Fig. 26(a) and (b), respectively. The parameter input follows a Gaussian distribution, with an uncertainty or so-called coefficient of variation (CV) of up to 70 % which is from the CV statistics in the famous paper by Duncan (2000) and the latest report of Ching et al. (2021). The figure shows how subsidence predictions evolve over time with a very high initial input CV, revealing greater variability (wider distribution) in the early years and decreasing variability (narrower distribution) as time progresses. The declining CV reflects a reduction in uncertainty over time, with the uncertainty of the subsidence output decreasing by nearly half by year 15 (CVyear15 = 0.369) and continuing to decline thereafter. From this calculation, it can be concluded that the settlement calculation of this parameter in the model exhibits a significant reduction in uncertainty.

5. Conclusions

The following observations were made in the present study:

1) Structured soft clay with low permeability was found to be widely and deeply distributed in Kashiwazaki City of Niigata Prefecture based on the ground investigation.
2) The subsidence of the ground observed before the Niigata-ken Chuetsu-oki Earthquake of 2007 was mainly due to groundwater pumping in the winter season from the correlation between the fluctuations in the ground water table. However, no strong correlation between the fluctuations in the ground water table and the post-earthquake subsidence were observed.
3) It was confirmed from the results of the numerical simulation, based on the ground investigation, that highly structured soft clay causes long-term post-earthquake subsidence due to (a) the long-term dissipation of excess pore water pressure generated during a large-scale earthquake and (b) the further degradation of the structure of clay during the post-earthquake consolidation process. The characteristics are outstanding for highly structure-susceptible soft clay with weathered seashells present in the deep layer compared to the less structured soft clay in the shallow layer, meaning the large potential for long-term post-earthquake subsidence and high susceptibility to damage of the structure in the deep layer.
4) In addition, based on the results of the numerical simulation, it was also found that the value of C_d (compression index induced by dynamic loading) for the deep layer was greater than that for the shallow layer. However, it decreased a little with the increase in OCR, which is consistent with the conclusion of Ohara and Matsuda (1988).
5) According to the simulation results using the limited information, it was predicted that the dissipation of excess pore water pressure and ground subsidence would last for more than 100 years after the earthquake. Although further investigation is necessary to verify the conclusions, because they are influenced by various factors, such as the topographical distribution, drainage boundary, pumping in winter season, and so on, this study has clarified the important characteristics of structured soft clay during and after earthquakes.
6) Given the limited available test data, the ground structure was simplified for this paper. However, it is important to note that the data used in this study should ideally account for both spatial variability and variability in the test results. To address the limitations in terms of the ground information, conducting a sensitivity and spatial variation analysis of these parameters will be crucial. The authors are currently evaluating their impact and plan to present the findings in a future report. In the present study, only the permeability coefficient was examined, and the results of the sensitivity analysis indicated a significant reduction in uncertainty regarding ground settlement after ground motion in this model. The analysis of other parameters will be left for future research.

CRediT authorship contribution statement

Yazhou Jiang: Writing – review & editing, Writing – original draft, Visualization, Validation, Supervision, Software, Resources, Project administration, Methodology, Investigation, Formal analysis, Data curation, Conceptualization. **Koichi Isobe:** Writing – review & editing, Visualization, Validation, Supervision, Resources, Project administration, Methodology, Investigation, Funding acquisition, Formal analysis, Data curation, Conceptualization. **Satoru Ohtsuka:** Writing – review & editing, Supervision, Resources, Project administration, Investigation, Funding acquisition. **Toshiyuki Takahara:** Writing – review & editing, Supervision, Funding acquisition, Data curation.

Acknowledgements

The authors would like to sincerely acknowledge Mr. Yoshihito Nakano and Mr. Naofumi Suzuki of Kowa Corporation for their assistance with the field investigation. They also thank Prof. Zhang of Nagoya Institute of Technology for his support in relation to the simulation. Appreciation is also offered to Messrs. Yukitaka Iizuka and Masahiro Tomobuchi (former undergraduate students of Nagaoka University of Technology) for their contribution to the experimental and analytical study. This work was supported by JSPS KAKENHI Grant Numbers 26820190 and 16H02362.

References

Albano, M., Polcari, M., Bignami, C., Moro, M., Saroli, M., Stramondo, S., 2016. An innovative procedure for monitoring the change in soil seismic response by InSAR data: application to the Mexico City subsidence. Int. J. Appl. Earth Obs. Geoinf. 53, 146–158.

Asaoka, A., Nakano, M., Noda, T., 1994. Soil-water coupled behavior of saturated clay near/at critical state. Soils Found. 34 (1), 91–105.

Asaoka, A., Nakano, M., Noda, T., 2000a. Superloading yield surface concept for highly structured soil behavior. Soils Found. 40 (2), 99–110.

Asaoka, A., Nakano, M., Noda, T., Kaneda, K., 2000b. Delayed compression/consolidation of naturally clay due to degradation of soil structure. Soils Found. 40 (3), 75–85.

Asaoka, A., Noda, T., Yamada, E., Kaneda, K., Nakano, M., 2002. An elasto-plastic description of two distinct volume change mechanics of soils. Soils Found. 42 (5), 47–57.

Avilés, J., Pérez-Rocha, L.E., 2010. Regional subsidence of Mexico City and its effects on seismic response. Soil Dyn. Earthq. Eng. 30 (10), 981–989.

Ching, J., Schweckendiek, T., 2021. State-of-the-art review of inherent variability and uncertainty in geotechnical properties and models. ISSMGE Tech. Committ. 304.

Duncan, J.M., 2000. Factors of safety and reliability in geotechnical engineering. J. Geotech. Geoenviron. Eng. 126 (4), 307–316.

Hashiguchi, K., 1989. Superloading surface model in unconventional plasticity. J. Solids Structures 25, 917–945.

Hashiguchi, K., Ueno, M., 1977. Elastoplastic constitutive laws of granular material, Constitutive Equations of Soils. In: Murayama, S. and Schofield, A. N. (Eds.), Proc. 9th ICSMFE., Spec. Ses. 9 Tokyo, JSSMFE, pp. 73-82.

Hashiguchi, K., Chen, Z.P., 1998. Elasto-plastic constitutive equations of soils with the subloading surface and the rotational hardening. Numer. Anal. Meth. Geomech. 22, 197–227.

Hashiguchi, K., 1978. Plastic constitutive equations of granular material. In: Cowin, S.C. and Satake, M. (Eds.), Proc. US-Japan Seminar on Continuum Mechanics and Statistical Approaches in the Mechanics of Granular-Materials. Sendai, JSSMFE. Pp. 321-329.

Hokuriku Geological System. https://www.hokuriku-jiban.info/.

Hyodo, M., Yasuhara, K., Hirao, K., 1988. Prediction of pore pressure and deformation in soft clay under long-term cyclic shear conditions. J. of JSCE. 400 (III-10), 151–160, in Japanese.

Hyodo, M., Yasuhara, K., Hirao, K., 1992. Prediction of clay behaviour in undrained and partially drained cyclic triaxial tests. Japanese Society of Soil Mechanics and Foundation Engineering. 32 (4), 117–127.

Isobe, K., Ohtsuka, S., Nunokawa, H., 2014a. Field investigation and model tests on differential settlement of houses due to liquefaction in the Niigata-ken Chuetsu-Oki Earthquake of 2007. Soils Found. 54 (4), 675–686.

Isobe, Y., Shahin, H.M., Nakai, T., 2014b. Effectiveness of reinforcement in embankment ground subjected to repeated shear deformation. J. GEOMATE. 7 (14), 1111–1116.

Jaime, A.P., Romo, M.P., Jasso, M.R., 1987. Seismic induced settlement in a building. 8Th Pan-American Congress on Soil Mechanics and Foundation Engineering, pp. 257–275.

Jiang, Y., Isobe, K., Ohtsuka, S., Takahara, T., 2024. Sensitivity analysis on long-term subsidence of soft clay due to The Niigata-ken Chuetsu-oki Earthquake in 2007. Japanese Geotechnical Society Special Publication. 10 (44), 1635–1640.

Kaneda, K., Yamada, S., Asaoka, A., 2003. Delayed compression observed in the land subsidence due to dewatering. J. of JSCE. 743 (III-64), 89–103, in Japanese.

Likitlersuang, S., Plengsiri, P., Mase, L.Z., Tanapalungkorn, W., 2020. Influence of spatial variability of ground on seismic response analysis: a case study of Bangkok subsoils. Bull Eng Geol Environ 79, 39–51.

Lysmer, J., Kuhlemeyer, R.L., 1969. Finite dynamic model for infinite media. J. Eng. Mech. Div. 95, 859–878.

Mase, L.Z., 2020. Seismic hazard vulnerability of bengkulu city, indonesia, based on deterministic seismic hazard analysis. Geotech Geol Eng 38, 5433–5455.

Mase, L.Z., 2021. Local site investigation and ground response analysis on downstream area of Muara Bangkahulu River, Bengkulu City, Indonesia. Indian Geotech. J. 51 (5), 952–966.

Mase, L.Z., Tanapalungkorn, W., Likitlersuang, S., Ueda, K., Tobita, T., 2022. Liquefaction analysis of Izumio sands under variation of ground motions during strong earthquake in Osaka, Japan. Soils Found. 62 (5) 101218.

Matsuda, H., Nagira, H., 2000. Decrease in effective stress and reconsolidation of saturated clay induced by cyclic shear. J. of JSCE. 659 (III-52), 63–75, in Japanese.

Matsuda, H., Ohara, S., 1990. Effects of loading period of cyclic shear on the settlement of saturated clayey layer. J. of JSCE. 418 (III-13), 173–179, in Japanese.

Matsuda, H., 1997. Estimation of post-earthquake settlement-time relations of clay layers. J. of JSCE. **568** (III-39), in Japanese.

Morikawa, Y., Bao, X., Maeda, K., Imase, T., Zhang, F., 2012. Importance of liquefaction analysis considering re-liquefaction due to aftershock of earthquake. Japanese Geotechnical Journal. 7 (2), 389–397.

Nakai, T., Hinokio, M., 2004. A simple elastoplastic model for normally and over consolidated soils with unified material parameters. Soils Found. 44 (2), 53–70.

Nigorikawa, N., Asaka, Y., 2015. Leveling of long-term settlement of Holocene clay ground induced by the 2011 off the Pacific coast of Tohoku earthquake. Soils Found. 55 (5), 1318–1325.

Ohara, S., Matsuda, H., 1988. Study on the settlement of saturated clay layer induced by cyclic shear. Soils Found. 28 (3), 103–113.

Ohtsuka, S., Isobe, K., Fukumoto, Y., 2021. Wide-area Land Subsidence of Kashiwazaki Plain due to the 2007 Niigata-ken Chuetsu-Oki Earthquake. Geotechnical Engineering Journal of the SEAGS & AGSSEA. 52 (4), 1–7.

Oka, F., Yashima, A., Kato, M., Sekiguchi, K., 1992. A constitutive model for sand based on the non-linear kinematic hardening rule and its application. In: Proc. 10th World Conf. Earthquake Engineering, Madrid, 5, Balkema. Pp. 2529–2534.

Oka, F., Yashima, A., Tateishi, A., Taguchi, Y., Yamashita, A., 1999. A cyclic elastoplastic constitutive model for sand considering a plastic-strain dependence of the shear modulus. Geotechnique 49 (5), 661–680.

Ovando-Shelley, E., Ossa, A., Santoyo, E., 2013. Effects of regional subsidence and earthquakes on architectural monuments in mexico city. Boletin De La Sociedad Geologica Mexicana. 65 (1), 157–167.

Qodri, M.F., Mase, L.Z., Likitlersuang, S., 2021. Non-linear site response analysis of bangkok subsoils due to earthquakes triggered by three pagodas fault. Eng. J. 25 (1), 43–52.

Roscoe, K.H., Schofield, A.N., Thurairajah, A., 1963. Yielding of clays in states wetter than critical. Geotechnique 13 (3), 211–240.

Schofield, A.N., Wroth, C.P., 1968. Critical state soil mechanics. McGraw-Hill.

Sekiguchi, H., 1977. Rheological characteristics of clays. Proc. 9^{th} ICSMFE., Tokyo, 1. Pp. 289-292.
Sento, N., 2020. Subsidence of clayey ground after an earthquake occurred in Iwaki City, Fukushima Prefecture and its generation mechanism. Japanese Geotech. J. 15 (4), 697–704, in Japanese.
Shogaki, T., Sakamoto, R., 2004. The applicability of a small diameter sampler with a two-chambered hydraulic piston for Japanese clay deposits. Soils Found. 44 (1), 113–124.
Si, H., Midorikawa, S., 1999. New attenuation relationships for peak ground acceleration and velocity considering effects of fault type and site condition. J. Struct. Constr. Eng. 523, 63–70.
Strong-motion Seismograph Networks (K-NET, KiK-net). National Research Institute for Earth Science and Disaster Resilience. https://www.kyoshin.bosai.go.jp/ (Reference date 2024-07-27).
Suzuki, T., 1984. Settlement of saturated clays under dynamic stress history. J. Jpn. Soc. Eng. Geol. 25 (3), 21–31, in Japanese.
Yashima, A., Oka, F., Shibata, T., Uzuoka, R., 1991. Liquefaction analysis by LIQCA. Proc. JGS Conference on Liquefaction of Ground and Its Counter Measure, pp. 165–174, in Japanese.
Yasuhara, K., Andersen, K.H., 1991. Clay behaviour under consecutive long-term cyclic loading in direct simple shear tests. J. of JSCE. 439 (III-17), 9–16, in Japanese.
Yasuhara, K., Yamanouchi, T., Hirao, K., 1982. Cyclic strength and deformation of normally consolidated clay. Soils Found. 22 (3), 77–91.
Ye, B., Ye, G., Zhang, F., Yashima, A., 2007. Experiment and numerical simulation of repeated liquefaction-consolidation of sand. Soils Found. 47 (3), 547–558.
Zeevaert, L., 1973. Foundation Engineering; For Difficult Subsoil Conditions, Second Edition, Van Nostrand Reinhold Company Inc., Pp. 521–523.
Zhang, F., Ye, B., Noda, T., Nakano, M., Nakai, K., 2007. Explanation of cyclic mobility of soils: Approach by stress-induced anisotropy. Soils Found. 47 (4), 635–648.